

EXPERIMENTAL AND COMPUTATIONAL FLUID  
DYNAMICS SIMULATION STUDIES ON DIRECT  
CONTACT MEMBRANE DISTILLATION IN DESALINATION

CHONG KOK CHUNG

MASTER OF ENGINEERING SCIENCE

FACULTY OF ENGINEERING SCIENCE  
UNIVERSITI TUNKU ABDUL RAHMAN  
SEPTEMBER 2014

**EXPERIMENTAL AND COMPUTATIONAL FLUID DYNAMICS  
SIMULATION STUDIES ON DIRECT CONTACT MEMBRANE  
DISTILLATION IN DESALINATION**

By

**CHONG KOK CHUNG**

A dissertation submitted to the Department of Chemical Engineering,  
Faculty of Engineering and Science,  
Universiti Tunku Abdul Rahman,  
in partial fulfillment of the requirements for the degree of  
Master of Engineering Science  
September 2014

*To my wonderful wife, Gee Chin,  
the finest people who I've ever met.*

## **ABSTRACT**

# **EXPERIMENTAL AND COMPUTATIONAL FLUID DYNAMICS SIMULATION STUDIES ON DIRECT CONTACT MEMBRANE DISTILLATION IN DESALINATION**

**Chong Kok Chung**

Membrane distillation (MD) was first patented in 1963, but only recently it became an interest of research in membrane separation process due to the advancement in membrane fabrication. It has been concluded that membrane materials and operating parameters play a vital role in the MD process to produce high permeate flux. In this study, the performance study of direct contact membrane distillation (DCMD) was conducted using self-fabricated polyvinylidene fluoride (PVDF) hollow fiber (HF) membranes with different types of additives, including ethylene glycol (EG), polyethersulfone (PES), surface modifying macromolecules (SMM) and lithium chloride (LiCl) to remove sodium chloride (NaCl) from synthesis seawater. Later, the membranes were tested under different operating parameters including temperature and flow rate. It was found that the PVDF membrane with EG and PES additives (PVDF-EG-PES) possessed the highest permeate flux. The feed inlet temperature had a positive on the permeate flux for all the membranes was observed. Further investigation of the PVDF-EG-PES membrane under different feed and permeate inlet flow rates

revealed that both of the flow rates demonstrated a positive effect on the permeate flux. The range (2.92 to 14.12 kg/m<sup>2</sup>.hr) of permeate flux produced by the PVDF-EG-PES membrane was comparable to those reported in the literature. The stability test of 20 hours operating time revealed that the PVDF-EG-PES membrane was able to produce a consistent permeate flux and superior rejection rate throughout the operation. Meanwhile, the thermal efficiency result indicated the increase of feed inlet temperature, feed and permeate inlet flowrates was able to increase the thermal efficiency of the DCMD process (from 54 to 76%). In addition to the experimental studies, computational fluid dynamics (CFD) simulation was also adopted in this study due to its potential in designing the DCMD process prior to the experimental study for time reduction and better understanding of the heat transfer behavior of the system. Good agreement between the experimental and CFD simulation results of inlet and outlet temperatures was clearly observed.

## ACKNOWLEDGEMENT

First of all, a great thank to Universiti Tunku Abdul Rahman (UTAR) in sponsoring my master of engineering science studies and Professor Ahmad Fauzi from Universiti Teknologi Malaysia (UTM) for his generosity assistance throughout the research.

I indebted and grateful to my dearest supervisor who is also deputy dean in Faculty of Engineering and Science, Dr Lai Soon Onn, for his relentless patience and support until the completion of this research.

Thousand thanks to Dr Lee Khia Min, the co-supervisor, Dr Lau Woei Jye from UTM, Dr. Ooi Boon Seng from Universiti Sains Malaysia (USM) and Dr. Lau Kok Keong from Universiti Teknologi Petronas (UTP) for their guidance throughout. I would like to express my deep appreciation to laboratory staffs from UTAR, UTM and USM for their unknowing, yet remarkable, contribution to this work.

I owe much gratitude to my parent and my wife for their constant encouragement throughout and beyond this works, without them, this work have ended somewhere before this page.

*This research work is financially supported by UTAR research grant (vote no: 6200/C30).*

## APPROVAL SHEET

This dissertation/thesis entitled **“EXPERIMENTAL AND COMPUTATIONAL FLUID DYNAMICS SIMULATION STUDIES ON DIRECT CONTACT MEMBRANE DISTILLATION IN DESALINATION”**

was prepared by CHONG KOK CHUNG and submitted as partial fulfillment of the requirements for the degree of Master of Engineering Science Structure A at Universiti Tunku Abdul Rahman.

Approved by:

---

(Assistant Prof. Dr. Lai Soon Onn)  
Supervisor  
Department of Chemical Engineering  
Faculty of Engineering and Science  
Universiti Tunku Abdul Rahman

Date : 3<sup>rd</sup> September 2014

---

(Assistant Prof. Dr. Lee Khia Min)  
Co-supervisor  
Department of Civil Engineering  
Faculty of Engineering and Science  
Universiti Tunku Abdul Rahman

Date : 3<sup>rd</sup> September 2014

**FACULTY OF ENGINEERING SCIENCE**

**UNIVERSITI TUNKU ABDUL RAHMAN**

Date: 3<sup>rd</sup> September 2014

**SUBMISSION OF DISSERTATION**

It is hereby certified that **Chong Kok Chung** (ID No: **11UEM05531**) has completed this dissertation entitled “*Experimental and Computational Fluid Dynamics Simulation Studies on Direct Contact Membrane Distillation in Desalination*” under the supervision of Dr. Lai Soon Onn (Supervisor) from the Department of Chemical Engineering, Faculty of Engineering and Science, and Dr. Lee Khia Min (Co-Supervisor) from the Department of Civil Engineering, Faculty of Engineering and Science.

I understand that University will upload softcopy of my dissertation in pdf format into UTAR Institutional Repository, which may be made accessible to UTAR community and public.

Yours truly,

---

(*Chong Kok Chung*)

## DECLARATION

I hereby declare that the dissertation is based on my original work except for quotations and citations which have been duly acknowledged. I also declare that it has not been previously or concurrently submitted for any other degree at UTAR or other institutions.

---

Chong Kok Chung  
Date : 3<sup>rd</sup> September 2014

## TABLE OF CONTENTS

	<b>Page</b>
<b>DEDICATION</b>	
<b>ABSTRACT</b>	<b>ii</b>
<b>ACKNOWLEDGEMENT</b>	<b>iv</b>
<b>APPROVAL SHEET</b>	<b>v</b>
<b>SUBMISSION OF DISSERTATION</b>	<b>vi</b>
<b>DECLARATION</b>	<b>vii</b>
<b>TABLE OF CONTENTS</b>	<b>viii</b>
<b>LIST OF TABLES</b>	<b>xi</b>
<b>LIST OF FIGURES</b>	<b>xii</b>
<b>LIST OF ABBREVIATIONS</b>	<b>xv</b>
<b>LIST OF NOTATIONS</b>	<b>xvii</b>
<b>CHAPTER</b>	
<b>1.0 INTRODUCTION</b>	<b>1</b>
1.1 Problem Statement	2
1.2 Aim and Objectives	3
1.3 Outline of the Dissertation	4
<b>2.0 LITERATURE REVIEW</b>	<b>6</b>
2.1 Overview of Desalination	6
2.2 Membrane Distillation (MD)	8
2.2.1 History of MD	8
2.2.2 Principle of MD	9
2.2.3 Configurations of MD	10
2.2.3.1 DCMD	11
2.2.3.2 AGMD	12
2.2.3.3 SGMD	12
2.2.3.4 VMD	13
2.2.4 Membrane Modules	13
2.2.4.1 Flat Sheet Membrane Module	14
2.2.4.2 Spiral Wound Membrane Module	14
2.2.4.3 Hollow Fiber Membrane Module	15
2.2.5 Effect of Membrane Characteristics on MD Process	16
2.2.6 Effect of Membrane Dope Solution on MD Process	19
2.2.7 Effect of Operating Parameters on MD Process	23
2.3 Computational Fluid Dynamics (CFD)	24
2.3.1 Fundamentals	24
2.3.2 Advantages of CFD in DCMD Simulation Study	29
2.4 Heat Transfer in MD	32

<b>3.0</b>	<b>METHODOLOGY</b>	<b>37</b>
3.1	Membrane Fabrication	37
3.1.1	Materials	37
3.1.2	Preparation of Dope Solution	37
3.1.3	Spinning of HF Membrane	38
3.2	Membrane Characterization Techniques	39
3.2.1	Membrane Morphology	39
3.2.2	Porosity	40
3.2.3	Contact Angle	41
3.2.4	Liquid Entry Pressure	42
3.3	Experiment Setup	43
3.4	CFD Simulation	46
3.4.1	Development of CFD Model	46
3.4.2	Grid Independence Analysis	49
<b>4.0</b>	<b>RESULTS AND DISCUSSION</b>	<b>51</b>
4.1	DCMD Experimental Study	51
4.1.1	Membrane Characteristics	51
4.1.1.1	Membrane Morphology	51
4.1.1.2	Membrane Thickness	56
4.1.1.3	Membrane Porosity and Pore Size Distribution	56
4.1.1.4	Membrane Contact Angle	60
4.1.1.5	Membrane Liquid Entry Pressure	60
4.1.2	Effect of Temperature on DCMD Performance	61
4.1.3	Effect of Flow Rate on DCMD Performance	63
4.1.4	Membrane Stability Test	65
4.1.5	Analysis of Thermal Efficiency	67
4.2	CFD Simulation Study	70
4.2.1	Temperature Distribution Analysis	70
<b>5.0</b>	<b>CONCLUSIONS AND RECOMMENDATIONS</b>	<b>75</b>
5.1	Conclusions	75
5.2	Recommendations	77
	<b>REFERENCES</b>	<b>79</b>
	<b>APPENDICES</b>	
A	Membrane Porosity Calculation	86
B	Membrane Contact Angle Measurement	88
C	Membrane Liquid Entry Pressure Measurement	92
D	Effect of Temperature on DCMD Performance	93
E	Effect of Flow Rate on DCMD Performance	94
F	Membrane Stability Test	95
G	Data Input in Fluent ® Software	97



## LIST OF TABLES

<b>Table</b>		<b>Page</b>
2.1	Effect of membrane parameter on permeate flux production in DCMD	19
2.2	Effect of operating parameter on permeate flux production in DCMD	24
3.1	Composition of spun membrane	38
3.2	Spinning parameters of HF membrane	39
3.3	Boundary conditions of 2D geometry model	48
3.4	Grid independence analysis based on feed outlet velocity (m/s)	50
4.1	Self-fabricated membrane thickness	56
4.2	Self-fabricated membrane porosity and mean pore size	57
4.3	Self-fabricated membrane contact angle	60
4.4	Self-fabricated membrane liquid entry pressure	61
4.5	The feed outlet temperature comparison between experimental and CFD simulation studies (Feed and permeate inlet flow rate each at 0.3 L/min)	71
4.6	The permeate outlet temperature comparison between experimental and CFD simulation studies (Feed and permeate inlet flow rate each at 0.3 L/min)	71

## LIST OF FIGURES

<b>Figures</b>		<b>Page</b>
2.1	Distribution of earth water	6
2.2	World water stress indicators	7
2.3	Direct contact membrane distillation	10
2.4	Type of membrane distillation	11
2.5	Flat sheet membrane module	14
2.6	Spiral wound membrane module	15
2.7	Hollow fiber membrane module	16
2.8	Effect of amount of LiCl additive in the PVDF-LICL-DMA membrane on membrane porosity	20
2.9	Effect of amount of LiCl additive in the PVDF-NMP membrane on the permeate flux in ultrafiltration	21
2.10	Permeate flux benchmarking of hollow fiber membrane made with 12 wt% PVDF/ 88wt% NMP and 12 wt% PVDF/ 80 wt% NMP/ 8 wt% EG	22
2.11	SMM additive migration during membrane formation	23
2.12	Overview of CFD Modeling	26
2.13	CFD simulation result in VMD	31
2.14	Temperature distribution and velocity flow field for the DCMD setup with and without baffles	32
2.15	Heat transfer in DCMD	33
3.1	Scanning electron microscope	40
3.2	Contact angle goniometer	42
3.3	Schematic diagram of liquid entry pressure test	43

## LIST OF FIGURES

Figures		Page
3.4	Schematic diagram of DCMD system setup	45
3.5	2D geometry model of the membrane module	46
3.6	2D geometry model with 1 : 0.5 mesh size (10120 cell size)	47
3.7	2D geometry model with boundary type	47
4.1	Cross sectional SEM image of PVDF-NMP	52
4.2	Cross sectional SEM image of PVDF-EG	52
4.3	Cross sectional SEM image of PVDF-EG-PES	53
4.4	Cross sectional SEM image of PVDF-SMM	54
4.5	Cross sectional SEM image of PVDF-DMAC	55
4.6	Cross sectional SEM image of PVDF-LiCl	55
4.7	Pore size distributions for (a) PVDF-NMP (b) PVDF-EG (c) PVDF-EG-PES (d) PVDF-SMM (e) PVDF-DMAC (f) PVDF-LiCl	59
4.8	Membrane permeate flux as a function of feed inlet temperature with the operating condition of feed inlet flow rate = 0.3 L/min, permeate inlet flow rate = 0.3 L/min and permeate inlet temperature = 18 °C	62
4.9	Membrane permeate flux as a function of feed inlet flow rate with the operating condition of feed inlet temperature = 55 °C, permeate inlet flow rate = 0.3 L/min and permeate inlet temperature = 18 °C	63
4.10	Membrane permeate flux as a function of permeate inlet flow rate with the operating condition of feed inlet temperature = 55 °C, feed inlet flow rate = 0.6 L/min and permeate inlet temperature = 18 °C	64

## LIST OF FIGURES

<b>Figures</b>		<b>Page</b>
4.11	Membrane stability test under feed inlet temperature (55°C) and permeate inlet temperature (18 °C) at different stream flow rates (a) feed and permeate inlet flow rate at 0.3 L/min respectively (b) feed and permeate inlet flow rate at 0.6 L/min respectively	66
4.12	Thermal efficiency with a function of feed inlet temperature	68
4.13	Thermal efficiency with a function of feed inlet flow rate	69
4.14	Thermal efficiency with a function of permeate inlet flow rate	69
4.15	Temperature distribution in the membrane module (a) feed inlet temperature at 40 °C (b) feed inlet temperature at 45 °C (c) feed inlet temperature at 50 °C (d) feed inlet temperature at 55 °C	74

## LIST OF ABBREVIATIONS

2D	Two dimensional
AGMD	Air gap membrane distillation
CFD	Computational fluid dynamics
DCMD	Direct contact membrane distillation
DMAC	N,N-dimethylacetamide
EG	Ethylene glycol
FVM	Finite volume method
HF	Hollow fiber
ID	Inner diameter
LEP	Liquid entry pressure
LiCl	Lithium chloride
MD	Membrane distillation
NaCl	Sodium chloride
NF	Nanofiltration
NMP	1-methyl-2-pyrrolidone
OD	Outer diameter
PDE	Partial differential equation
PE	Polyethylene
PES	Polyethersulfone
PIV	Particle image velocimetry
PP	Polypropylene
PTFE	Polytetrafluoroethylene
PVDF	Polyvinylidene fluoride
RO	Reverse osmosis
SEM	Scanning electron microscope

## LIST OF ABBREVIATIONS

SGMD	Sweeping gas membrane distillation
SIMPLE	Semi-implicit method for pressure linked equation
SMM	Surface modifying macromolecules
UF	Ultrafiltration
VMD	Vacuum membrane distillation

## LIST OF NOTATIONS

$wt\%$	Weight percent
$h_f$	Heat transfer coefficient of the feed solution
$h_m$	Heat transfer coefficient of the membrane
$h_p$	Heat transfer coefficient of permeate
$C_f$	Feed concentration
$C_p$	Permeate concentration
$Q_c$	Heat conduction across the membrane materials
$Q_f$	Heat transfer on feed side
$Q_m$	Heat transfer which involves the movement of the vapor across from the feed side of the membrane to permeate side
$Q_v$	Latent heat of vaporization
$T_{f,m}$	Feed/membrane interface temperature
$T_f$	Feed temperature
$T_{p,m}$	Permeate/membrane interface temperature
$T_p$	Permeate temperature
$W_1$	Weight of the wetted membrane
$W_2$	Weight of dry membrane
$c_p$	Specific heat
$k_g$	Thermal conductivity of membrane material
$k_p$	Thermal conductivity of gas
$\rho_w$	Specific gravity of 2-butanol
$\rho_b$	Specific gravity of PVDF
$\Delta H_{v,w}$	Latent heat of vaporization
$\Delta t$	Sampling time
$J$	Permeate flux

## LIST OF NOTATIONS

$R$	Rejection rate
$i$	Internal energy
$k$	Thermal conductivity
$p$	Pressure
$q$	Heat conduction
$u$	$x$ -direction velocity
$v$	$y$ -direction velocity
$w$	$z$ -direction velocity
$\delta$	Thermal conductivity of pore
$\varepsilon$	Porosity
$\eta$	Thermal efficiency
$\mu$	Viscosity
$\rho$	Density
$\tau$	Viscous stress

## CHAPTER 1

### INTRODUCTION

One of the major problems that the world is now facing is the scarcity of the potable water. About 70% of the earth surface is composed of water. Nevertheless, out of 96.5% of this water is held by ocean which is unsuitable for drinking (The USGS Water Science School, 2013). Membrane technology was broadly used in desalination plants around the world recently due to the maturity of the technology. On the other hand, membrane distillation is still a comparatively new technology relative to other techniques such as reverse osmosis (RO) due to its unique method of thermal separation. Nevertheless, the high rejection efficiency and possibility of integration with renewable energy are attracting the attention from both academic and industry (Tomaszewska, 2000; Bourawi et al., 2006; Alkhudhiri et al., 2012).

The membrane distillation (MD) is a thermal driven process in which only the feed vapor is transported through the pore of hydrophobic membrane, whereas the high surface tension force restricts the feed liquid from entering the permeate regime. The feed vapor will be condensed in the permeate stream and forming pure water distillate (Lawson and Lloyd, 1997). Direct contact membrane distillation (DCMD) is one of the most studied techniques by academic and industry in the desalination due to the simplicity of the experimental setup and a

promising heat and mass transfer characteristic (Bourawi et al., 2006, Al-Obaidani et al., 2008).

Computational fluid dynamics (CFD) is a numerical simulation analysis of fluid mechanics system which involves fluid flow, thermodynamic and heat transfer. CFD simulation has its advantages compared to experiment based approach to fluid system design such as reduction of lead time in new design, ability to study the system under dangerous conditions and ability to perform practically unlimited level of detailed studies (Versteeg and Malalasekera, 1995).

## **1.1 Problem Statement**

There are a few membrane based separation techniques used in desalination nowadays. Of these techniques, most of the desalination plants built in the world are adopting RO technique. It is worth noting that the RO process is a pressure driven separation process which involves high pressure as driving force for separation, and therefore high energy consumption is required. Unlike pressure driven processes, MD is a thermal driven process in nature where the heat source can be obtained from renewable energy and high rejection rate. Due to the advantages of MD in separation, an in depth study is essential for it to be commercially feasible.

The two significant factors governing the DCMD performance are membrane material and operating parameters. To date, various studies of DCMD have been performed based on the commercially available membranes used for other membrane processes. In view of that, a self-fabricated membrane that is specifically characterized for the requirements of DCMD system is important for a high permeate flux performance. Furthermore, the operating parameters such as fluid temperature and flow rate play an essential role as well to achieve a high performance DCMD system.

Meanwhile, the mathematical modeling of fluid flow phenomenon in DCMD with different membranes and operating parameter required an extensive time to be performed. Hence, CFD analysis is a useful tool that is less time consuming technique to predict the fluid flow phenomenon in the DCMD process.

## **1.2 Aim and Objectives**

The aim of this research project was to self-fabricate and characterize hollow fiber (HF) membrane with different additives which was subsequently applied in the DCMD system for sodium chloride removal.

The objectives of this research project can be summarized as follows:

1. To fabricate and characterize HF membranes using different additives in the spinning dope solution.

2. To determine the permeate flux of self-fabricated membranes under different feed and permeate inlet temperatures.
3. To investigate the effect of both feed and permeate flow rate on the membrane which possessed the highest permeate flux from the result in the study of the effect of different feed and permeate inlet temperatures.
4. To examine the stability of the membrane under longer operating duration.
5. To determine and evaluate thermal efficiency of the DCMD system.
6. To conduct a numerical simulation study using CFD technique in the analysis of membrane module temperature distribution.

### **1.3 Outline of the Dissertation**

Chapter 2 is the literature review which presents the comprehensive literature findings and comments on MD and CFD.

Chapter 3 describes the methodology of the experimental and simulation study. The in depth description of the membrane fabrication and characterization, experimental setup as well as the CFD simulation modeling will be discussed.

Chapter 4 demonstrates the results and discussion of the current research project. In this chapter, the results from both experimental and CFD simulation study will be presented.

Chapter 5 concludes the result of the current study together with the recommendations for future works

## CHAPTER 2

### LITERATURE REVIEW

#### 2.1 Overview of Desalination

Majority of the water source in the world is seawater which makes up of 96.5% of total water coverage. Figure 2.1 illustrates the amount of the water contained in the earth (The USGS Water Science School, 2013). Identically around the world, the average seawater salinity is about 3.5 wt% of sodium chloride (NaCl) which is translated to 35 grams of dissolved salt per one kilogram of seawater. It has been known not suitable for human consumption due to the high salinity content (Swenson, n.d.).

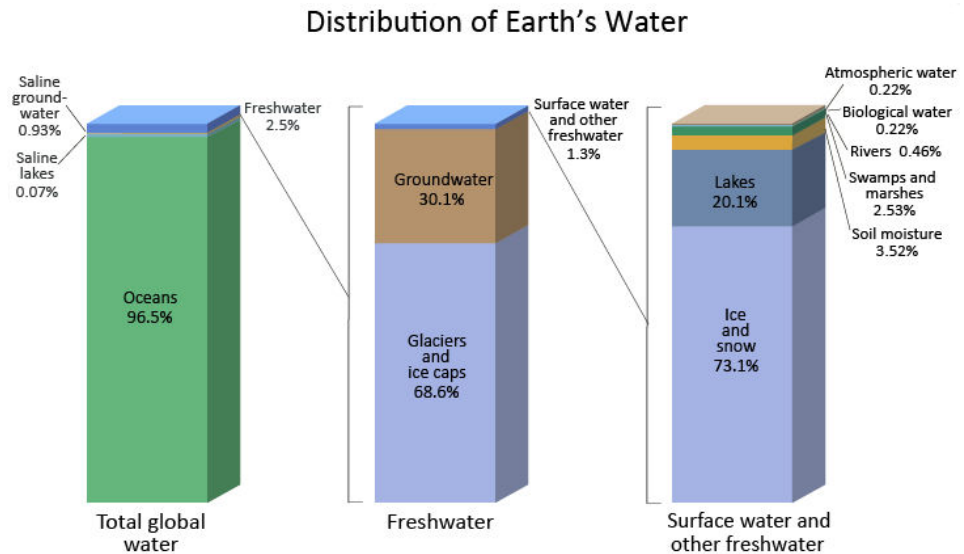


**Figure 2.1 Distribution of Earth Water (The USGS Water Science School, 2013)**

One of the major problems in the world facing now is the scarcity of the drinking water. According to the report from World Health Organization (2014), there is approximately 1.1 billion or one out of six of the human populations are out of reach of water. Everyday in the world, there are 5,000 of lives are claimed due to the water related contamination leading to serious diarrhea and majority of them are children. Nevertheless, many fresh water sources in the world are heavily polluted such as the discharge of toxic wastewater to the river. These harmful components in the wastewater, such as arsenic, cyanide, ammonia and mercury, are unsafe and will lead to serious health problem if they are consumed by human and affect the aquatic ecology (Qu et al., 2009; Xie et al., 2009). In addition, many countries are also facing the water stress due to the lack of fresh water supply in their population as shown in Figure 2.2.

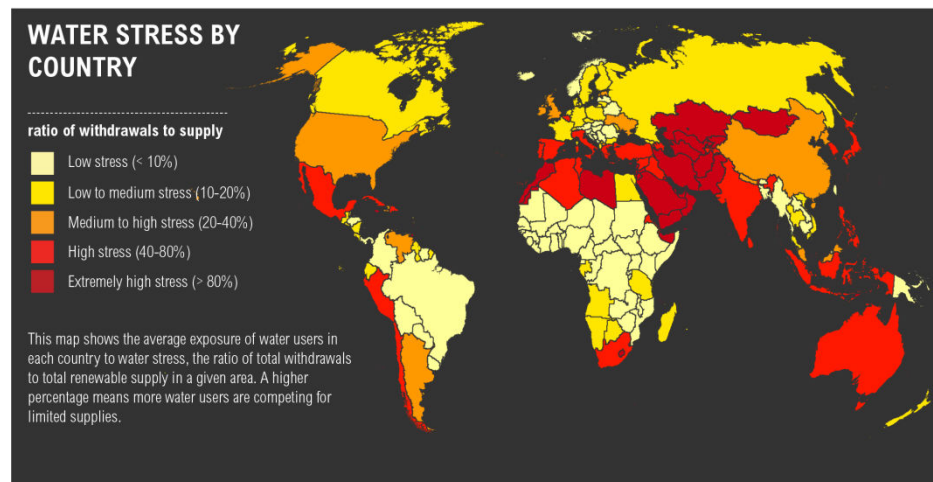


**Figure 2.2 World Water Stress Indicators (World Resources Institute, 2013)**

As the technology advancement in water separation technique, several desalination methods were introduced and to date, membrane separation is widely adopted in desalination. RO is a pressure driven membrane separation technique which is commonly used in desalination and approximately 56.5% of desalination plant is applying this method in freshwater production from seawater (Li et al., 2008). The range of pressure required in the separation of dissolved salt from seawater is 40 – 70 bar which leads to high energy consumption. Moreover, the RO has several other drawbacks on the operation, such as low back pressure as most of the pressure lost by discharging the wastewater to the reservoir and high energy consumption as it requires a high pressure driving forces. Therefore, many alternative techniques are proposed with the aim of reducing energy consumption by integrating low grade waste heat from electric generation plant and/or solar energy (Susanto, 2011). Among several membrane separation techniques in desalination, one of the recently emerging technologies is membrane distillation (MD) which adopts thermal driven forces and will be discussed in the following section.

## **2.2 Membrane Distillation (MD)**

### **2.2.1 History of MD**

The MD patent was first filed in America by Bodell who used silicon rubber as MD membrane in desalination. Few years after the MD concept was introduced by Bodell, Findley published the first journal paper in 1967 by

adopting DCMD technique in separation (Khayet and Matsuura, 2011). Nevertheless, MD popularity had been losing due to the difficulties in producing a good MD membrane and low permeate flux relative to other technique such as RO. The interest in MD was only recovered in the early 1980s due to the advancement in membrane fabrication technique which enabled the production of novel membrane with good MD membrane characteristics (Bourawi et al., 2006).

### **2.2.2 Principle of MD**

MD is a thermal driven membrane separation process which the feed vapor transport across the hydrophobic membrane and the vapor will be condensed by the permeate solution to produce pure water distillate. Figure 2.3 shows the working principle of the DCMD (Lawson and Llyod, 1997; Tomaszewska, 2000; Bourawi et al., 2006). Firstly, the feed solution is heated above room temperature and below the boiling point of the solution causing it change from liquid phase to liquid-vapor coexist phase as the result of increasing thermal energy in the solution. The thermal driving force in the feed solution will be exerted to the feed vapor for it to be transported towards the permeate stream through the pore of hydrophobic membrane. The feed liquid will be restricted from entering the permeate solution by the surface tension force on the membrane and remained at the origin. The water vapor will be condensed to pure water distillate in the permeate solution.

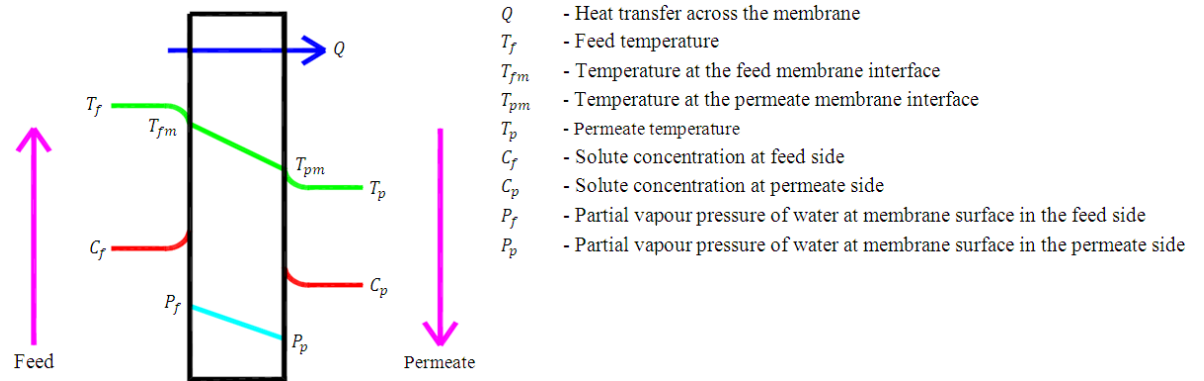


**Figure 2.3 Direct Contact Membrane Distillation**

### 2.2.3 Configurations of MD

There are several configurations of MD in acquiring the vapor pressure driving forces (Khayet and Matsuura 2011). In all of these configurations, liquid-vapor feed solution is directly exposed to the membrane, whereas the condensation techniques of permeate are different. Basically, the condensation methods of the permeate side can be distinguished to direct contact membrane distillation, vacuum membrane distillation, sweeping gas membrane distillation and air gap membrane distillation as shown in Figure 2.4.

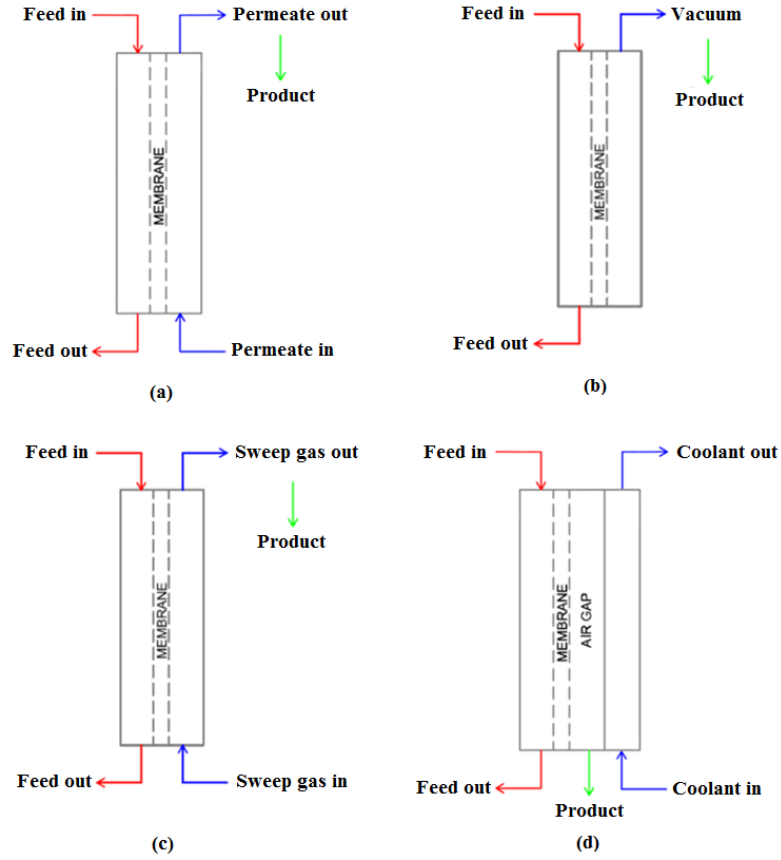


**Figure 2.4 Types of Membrane Distillation a) Direct Contact Membrane Distillation (DCMD) b) Vacuum Membrane Distillation (VMD) c) Sweeping Gas Membrane Distillation (SGMD) d) Air Gap Membrane Distillation (AGMD)**

### 2.2.3.1 DCMD

DCMD is the most popular configuration relative to the rest of the setup in MD due to its simplicity in setting up and providing optimum flux (Bourawi et al., 2006). To date, DCMD has been studied in desalination, fruit juice extraction and wastewater treatment. The feed and permeate solutions will be in direct contact which is separated by a porous hydrophobic membrane. Feed and permeate solution will be circulated either in parallel or counter flow by pump or stirrer.

The difference in vapor pressure between the heated feed and cold permeate solution enable the feed water vapor to transport across the membrane layer into permeate regime. Pure water distillate will be obtained as a result from the condensation of feed water vapor in the permeate solution.

### **2.2.3.2 AGMD**

AGMD (Khayet and Matsuura 2011) configuration is similar to DCMD with an additional air gap between feed and permeate solution. In AGMD, the feed water vapor transport across the hydrophobic membrane into the air gap which will be condensed by a cold water layer next to the air gap. The pure water permeate will be collected as an end product. Similar to DCMD, AGMD has garnered the interest of researchers in various water separation processes. Few of notable researches (Banat, 2007) are solar driven AGMD pilot plant in the Northern part of Jordan by Jordan University Science and Technology and solar driven desalination pilot plant in Gran Canaria, Northwestern coast of Africa.

### **2.2.3.3 SGMD**

SGMD (Bourawi et al., 2006) is the least studied MD technique due to the system complication and cost involved as it requires an external sweeping gas agent serving as condenser. Similar to DCMD, the feed solution will be heated until a liquid-vapor stage is reached. The vapor will be transferred to the permeate regime as the increase of vapor pressure. The condensate medium used in SGMD

is inert gas which acts as sweeping gas agent to sweep through feed vapor molecule on the pore of hydrophobic membrane. The vapor will be then condensed by external condenser attached to the system.

#### **2.2.3.4 VMD**

In VMD, this technique employs a vacuum or low pressure exerted to the permeate side by vacuum pump. The applied vacuum pressure forms a negative pressure on permeate and it enables the volatile molecules in vapor to be separated from feed. The condensation of these volatile molecules vapor will take place at the outside of the membrane module as a result of temperature difference (Khayet and Matsuura 2011). A number of researchers have been employing the VMD technique in their researches to remove certain substances in wastewater treatment. For instance, Zhao et al. (2007) removed 2,4-dichlorophenol which is commonly used in pesticide from the wastewater and Bing et al. (2006) remove 1,1,1-trichloroethane from water using PVDF membrane.

#### **2.2.4 Membrane Modules**

The design of the membrane module can be basically classified into three categories which are flat sheet, spiral wound and hollow fiber membrane modules. The design principles of these membrane modules are permitting high permeate flow with high membrane packing density, allowing good flow condition to avoid high pressure drop, good heat recovery function and excellence

in thermal stability to prevent heat loss (Li et al., 2008; Khayet and Matsuura 2011).

#### 2.2.4.1 Flat Sheet Membrane Module

Flat sheet membrane module was the first design in the MD system due to the ease of the module setup. Figure 2.5 shows a design of a flat sheet membrane module used in removal of arsenic contaminated groundwater by MD. The feed is flowing through one side of the module. Some of the vapor is transported across the membrane due to vapor pressure difference and the remaining feed will be re-circulated (Li et al., 2008; Khayet and Matsuura 2011).

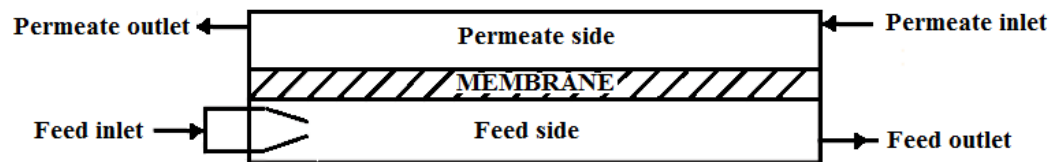


**Figure 2.5 Flat Sheet Membrane Module (Ajay et al., 2010)**

#### 2.2.4.2 Spiral Wound Membrane Module

Spiral wound module was first built for the artificial kidney design. But as the time evolves, spiral wound module is widely used in the membrane separation system such as MD. The design of the spiral wound module (Khayet and Matsuura 2011; Winter et al., 2011) consists of membrane envelope that is formed by a layer of membrane wound and spacer surrounding to a perforated permeate collection pipe as shown in Figure 2.6. The feed flows across the membrane

envelope in axial direction and some portions of the permeate vapor are compelled to the membrane envelope as there is vapor pressure difference. The permeate vapor flows spirally to the center of the module and exits through the perforated permeate collection pipe.

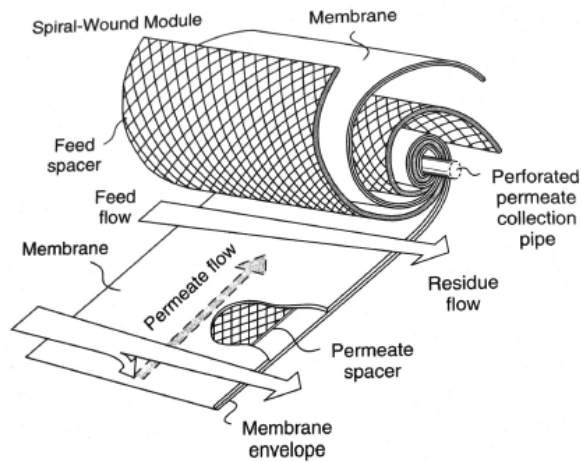


**Figure 2.6 Spiral Wound Membrane Module (Li et al., 2008)**

### 2.2.4.3 Hollow Fiber Membrane Module

Hollow fiber membrane module can basically be divided into two configurations (Li et al., 2008) which are shell side feed design and bore side feed design as shown in Figure 2.7. In the shell side feed design, membranes are bundled in a module. Feed solution flows from the shell side into the membrane module. With the increase of vapor pressure difference, the permeate is forced into the hollow fiber membrane and collected at one end, whereas the remaining feed solution will be re-circulated at the other end of the module. The advantage of the shell side feed design is large membrane area. The construction of the bore side feed design is similar to that of the shell side feed design, but the difference

is that the feed flows through the membrane instead of membrane module. Both ends of the membrane module are open for the recirculation of the feed solution. Permeate flows through the membrane by the driving force of vapor pressure difference.

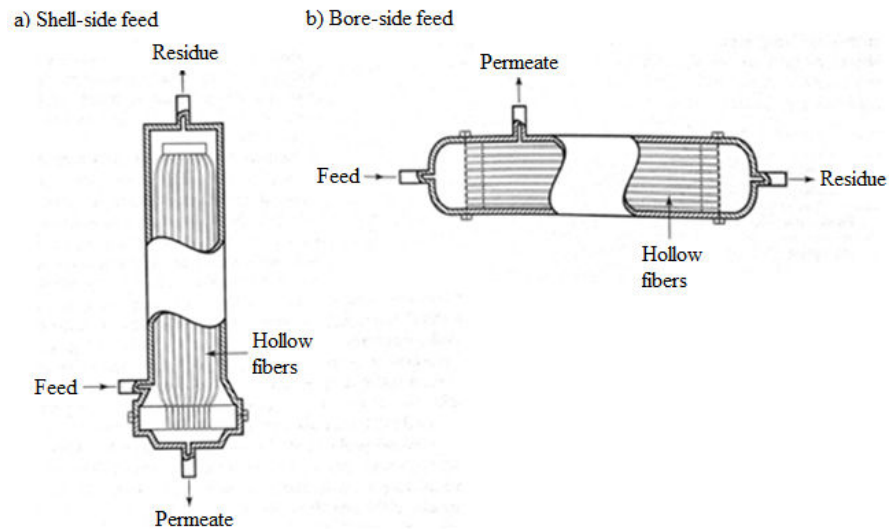


**Figure 2.7 Hollow Fiber Membrane Module Configurations a) Shell-side Feed Membrane Module b) Bore-side Feed Membrane Module (Li et al., 2008)**

### 2.2.5 Effect of Membrane Characteristics on MD Process

The membrane used in the MD process shall be porous hydrophobic membrane. However, some researchers combined the hydrophilic and hydrophobic characteristics into a dual layer membrane which has been tested in the MD and some lab-scale desalination system. Due to the technological advancement, several types of novel membranes such as composite membrane with ceramic and trilayer porous membrane were proposed compared to conventional single layer porous hydrophobic membrane (Bourawi et al., 2006).

As one of the requirements of MD membrane is non-wetted property by feed aqueous solution or having a hydrophobic characteristic, few notable polymer materials such as polytetrafluoroethylene (PTFE), polyethylene (PE), polypropylene (PP), and polyvinylidene fluoride (PVDF) were proposed by researchers in the fabrication of the MD membrane (Khayet, 2011). The selection of these polymer materials is based on its ability to produce an excellent hydrophobic, good thermal stability and fine chemical resistance characteristics membrane. Few investigations were conducted based on the performance of above polymers materials and the result showed that optimum fluxes were able to be obtained for both commercial available and lab fabricated membrane (Ahmad et al., 2013; Feng et al., 2013). Recently, several studies were carried out on the novel membranes for MD process, such as surface modifying macromolecules (SMM) membrane which showed the enhancement in permeate flux (Qtaishat et al., 2009).

Generally, a good membrane for MD shall be consisting of the following criteria (Bourawi et al., 2006; Khayet, 2011; Khayet and Matsuura 2011; Alkudhiri et al., 2012).

- A high porosity membrane with porosity in the range of 30 – 85%. Several researches showed permeate flux increased with the increase of pore distribution area of the membrane as a result of high porosity membrane permitting a lower conductive heat loss.

- Pore size in the membrane between 100 nm to 1  $\mu\text{m}$  will be enviable for the MD process. Besides, it is also able to avoid wettability of membrane pore as the liquid molecule is unable to pass through the small membrane pore.
- Thin membrane thickness will be desirable in the MD process as it is inversely proportional to the permeate flux. The optimum membrane thickness will be in the range of few micrometers to several hundred micrometers.
- Membrane tortuosity is a parameter that measures the fraction of the length of the membrane pore to membrane thickness. Membrane flux is inversely proportional to the product of membrane thickness and membrane tortuosity. Normally, the reported values of membrane tortuosity vary from 2 to 3.9, but to date there is no regular study on the effect of tortuosity as it is technically difficult to measure the real value.
- The membrane surface shall exhibit a strong chemical and fouling resistance. In general, one of the membrane surfaces will directly interface with the liquid-vapor to the feed solution in the DCMD process. As a result of this prolonged contact, membrane surface degradation and fouling may be arising.
- Membrane shall display a good thermal stability as the MD membrane will be extensively in contact with feed solution where the temperature is up to 100°C.

A summarized relationship between the membrane parameters and the on permeate flux in the DCMD is provided in Table 2.1.

**Table 2.1 Effect of Membrane Parameter on Permeate Flux Production in DCMD (Extracted from Bourawi et al., 2006)**

Membrane thickness	Porosity	Pore size	Pore size distribution
↓	↑	↑	↕

Note: ↑ : permeate flux increase with; ↓ : permeate flux decrease with; ↕ : very important may increase or decrease of permeate flux

### 2.2.6 Effect of Membrane Dope Solution on MD Process

Over the years in the MD membrane fabrication development, there were several investigations on the non-solvent additives added into the membrane dope solution in order to enhance the membrane characteristics for a better permeate flux (Feng et al., 2013). It is worthy to note that lithium chloride (LiCl), ethylene glycol (EG) and surface modifying macromolecule (SMM) are the additives that have been most studied due to their ability to improve the membrane characteristics.

Literally, LiCl is often referred as pore forming additive in the PVDF membrane fabrication. The ability of LiCl to increase the membrane porosity (as shown in Figure 2.8) is due to its characteristic to be dissolved rapidly when in contact with water which leads to the increase of diffusion rate of polymer solvent

from dope solution (Bottino et al., 1988; Tomaszewska, 1996). As a consequence, large cavities and porous structure were formed in the fabricated membrane, leading to the increment of permeate flux as shown in Figure 2.9 (Bottino et al., 1988)

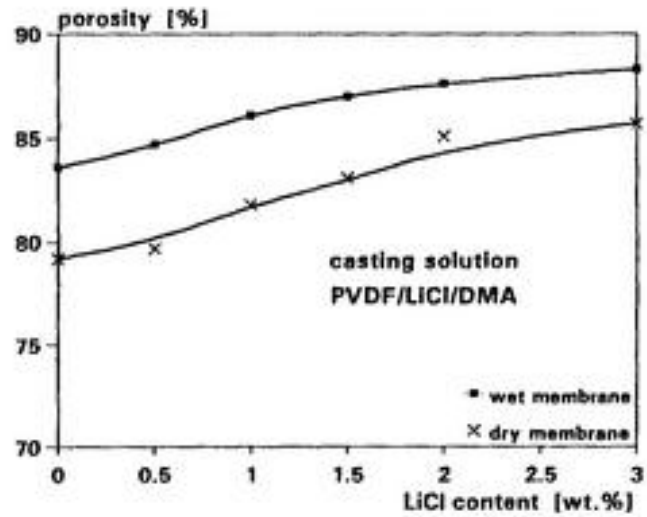


**Figure 2.8 Effect of Amount of LiCl Additive in the PVDF-LiCl-DMA Membrane on Membrane Porosity (Tomaszewska, 1996)**

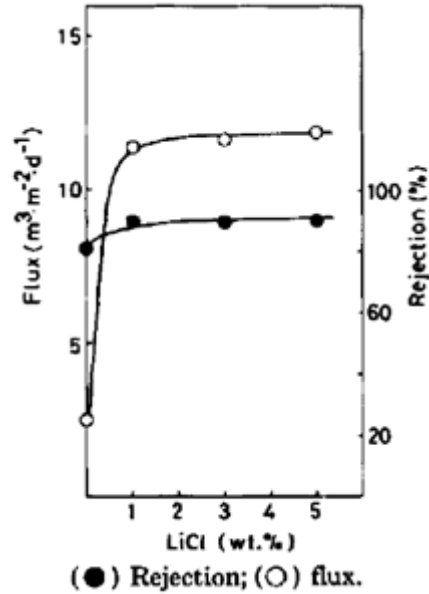


**Figure 2.9 Effect of Amount of LiCl Additive in the PVDF-NMP Membrane on the Permeate Flux in Ultrafiltration (Bottino et al., 1988)**

Wang et al. (2008) and Bonyadi et al. (2009) reported the functions of EG as non-solvent additive in membrane dope solution were to create a thin skin layer of membrane structure and to be involved in the rapid diffusion during phase separation. These studies found that a narrow pore size distribution could lead to the uniformity of the pores as well as the porosity of the membrane. Furthermore, membranes with an ultra skin layer thickness leads to the increase of permeate flux production in the MD process. Meanwhile, several studies reported the effect of the combination of PES and PVDF polymer on membrane fabrication. For instance, Zhang et al. (2009) discovered the improvement of membrane fouling resistance with optimum amount of polyethersulfone (PES) blended with PVDF. The study from Wang et al. (2008) indicated that the DCMD permeate flux

increased with the addition of EG in the PVDF hydrophobic membrane with NMP as solvent (Figure 2.10).

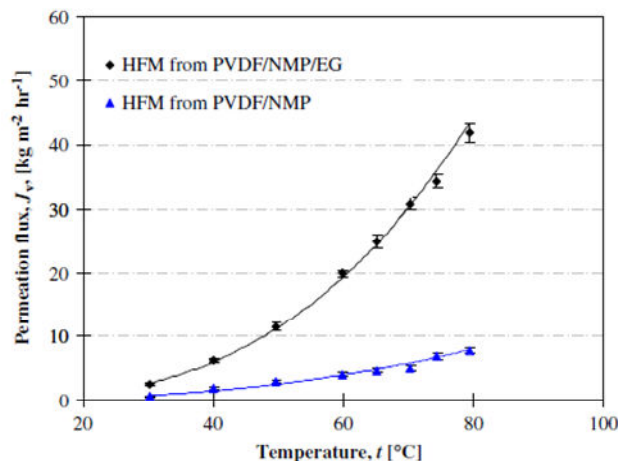


**Figure 2.10 Permeate Flux Benchmarking of Hollow Fiber Membrane Made with 12 wt% PVDF/ 88 wt% NMP and 12 wt% PVDF/ 80 wt% NMP/ 8 wt% EG (Wang et al., 2008)**

Recently, the interest of researchers is arising in the membrane fabrication integrated with hydrophobic SMM materials macromolecule with amphipathic structure of hydrophobic materials consisting of hydrophilic (polyurea or polyurethane) and hydrophobic (fluorine based polymer chain) parts (Suk et al., 2006; Sisakht et al., 2012). With this unique macromolecule structure, the surface properties of the membrane are changed by creating nano scale agglomerates on the surface as a result of migration of SMM materials to the membrane air interface. Figure 2.11 schematically illustrates the migration of SMM additive from membrane dope solution during the membrane formation (Essalhi & Khayet, 2012).

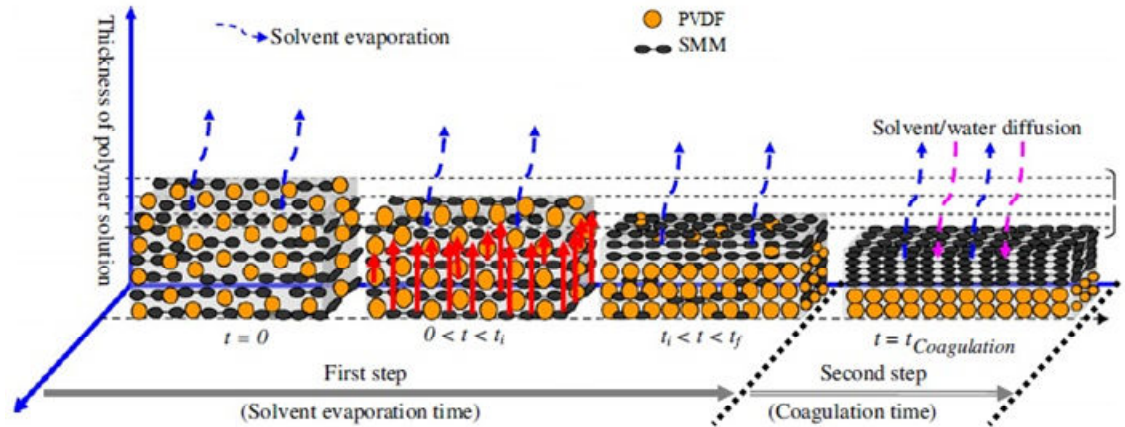


**Figure 2.11 SMM Additive Migration during Membrane Formation (Essalhi & Khayet, 2012)**

### 2.2.7 Effect of Operating Parameters on MD Process

As indicated in the Antoine equation, the vapor pressure increases exponentially with respect to the temperature. In view of that, there is a significant effect on the permeate flux which has been literally reported from previous works. According to the review of Bourawi et al. (2006), at a constant operation parameter of fluid flow rate and temperature, the permeate flux increased exponentially with the rise of feed inlet temperature, which denoted that the permeate flux in DCMD system strongly depended on the feed temperature. In the heat transfer study conducted by Qaishat et al. (2008) this phenomenon was attributed to the increase of temperature gradient between the feed and permeate solution, resulting in the increase in permeate flux.

In addition, feed and permeate flow rates also play a vital role in the permeate flux enhancement in the DCMD system. When the feed and permeate flow rates increase, the boundary layer resistance will be reduced and heat transfer coefficient will be increased, leading to the high permeate flux production (Termpiyakul et al., 2005). Therefore, the past MD studies showed that the permeate flux increase linearly with the rise of feed and permeate flow rate. The details of the effect of operating parameters on the permeate flux in DCMD are summarized in Table 2.2.

**Table 2.2 Effect of Operating Parameter on Permeate Flux Production in DCMD (Extracted from Bourawi et al., 2006)**

Variable		
Operating condition on feed solution, with effect of increasing of		
Temperature	Concentration	Velocity
↑	↓	↑
Operating condition on permeate solution, effect of increasing of		
Temperature	Concentration	Vapor pressure difference
↓	↑	↑

Note: ↑ : permeate flux increase with; ↓ : permeate flux decrease with;

## 2.3 Computational Fluid Dynamics (CFD)

### 2.3.1 Fundamentals

CFD is a method to numerically analyze a fluid flow system which is able to associate with chemical reaction, fluid dynamics, heat and mass transfer

(Versteeg and Malalasekera, 1995). CFD simulation applies the numerical analysis method which numerically approximates the mathematical model which governing the fluid flow phenomenon. As the nature of the numerical analysis, CFD is able to simplify the complicated model governing the membrane separation mechanism which enables the user to reduce the lead time in geometry model construction. With the capability of CFD in numerically solving the governing mathematical model, it enables the user to investigate the membrane separation phenomenon such as fluid flow (Shakaib et al., 2012; Yang et al., 2012). Whenever the computing facilities are available, CFD is able to perform almost unrestricted level of system details in the membrane separation and study the phenomenon where the controlled experiment is unable to be performed (Versteeg and Malalasekera, 1995).

Commercially available CFD software such as FLUENT® involves three main elements which can be categorized as pre-processor, solve and post processor as illustrated in Figure 2.12. The CFD code is basically a structured algorithm to numerically solving the mathematical model governing in the fluid flow phenomenon (Versteeg and Malalasekera, 1995). Pre-processor involves the transformation of a fluid problem into the CFD software through the geometry modeling. Subsequently, computational domain, meshing, materials properties and required boundary condition are defined on the geometry model before being exported to the solver. In the solver, FLUENT® applies finite volume method where the necessary governing equations in the fluid phenomenon will be

included into the cells of the computational domain. The governing equations will be solved by numerical iteration until the solution is converged. The final result will be presented in the graphical user interface in post-process for user in depth analysis (Versteeg and Malalasekera, 1995).

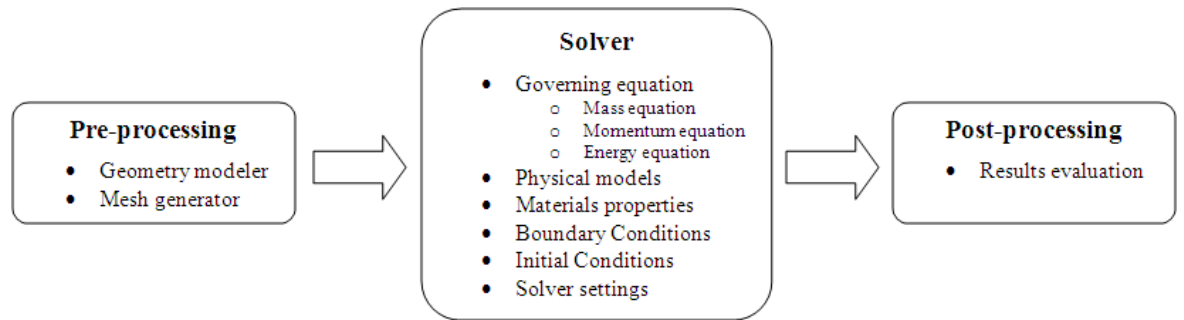


**Figure 2.12 Overview of CFD Modeling**

The governing equations in CFD which involves fluid flow and heat transfer are mathematically written from the conservation law of physics including the phenomenon of mass, momentum and energy.

The conservation of mass is described as the rate of increase in the movement of mass in the fluid element is equivalent to the net flow of mass into the fluid element in which the resulting mass balance is expressed in Equation 2.1,

$$\frac{\partial \rho}{\partial t} + \frac{\partial(\rho u)}{\partial x} + \frac{\partial(\rho v)}{\partial y} + \frac{\partial(\rho w)}{\partial z} = 0 \quad (2.1)$$

where  $\rho$  is the density,  $u, v, w$  are the  $x$ -,  $y$ - and  $z$ - direction velocity respectively.

The conservation of momentum is described by Newton's second law depicted that the rate of momentum increase in the fluid element is equivalent to the sum of exerted forces on the fluid element. The effects of the exerted forces on the fluid elements derived from Newton's second law in the CFD include pressure,  $p$  and viscous stresses,  $\tau$  exerted onto the surface of fluid element. Therefore, the stresses exerted on the fluid element per unit volume on  $x$ -direction can be expressed in Equation 2.2,

$$\frac{\partial(-p+\tau_{xx})}{\partial x} + \frac{\partial\tau_{yx}}{\partial y} + \frac{\partial\tau_{zx}}{\partial z} \quad (2.2)$$

Furthermore, the momentum equation can be expressed per unit volume basis including the source term,  $S$  contributions due to body forces (e.g. gravity) which can be summarized as the rate of change of momentum on the fluid elements equal to the sum of total forces exerted to the fluid element and rate of change of momentum due to source term. The momentum equations for the  $x$ ,  $y$  and  $z$ -direction are therefore expressed as follows,

$$x - direction : \rho \frac{Du}{Dt} = \frac{\partial(-p+\tau_{xx})}{\partial x} + \frac{\partial\tau_{yx}}{\partial y} + \frac{\partial\tau_{zx}}{\partial z} + S_{Mx} \quad (2.3)$$

$$y - direction : \rho \frac{Dv}{Dt} = \frac{\partial \tau_{xy}}{\partial x} + \frac{\partial(-p + \tau_{yy})}{\partial y} + \frac{\partial \tau_{zy}}{\partial z} + S_{My} \quad (2.4)$$

$$z - direction : \rho \frac{Dw}{Dt} = \frac{\partial \tau_{xz}}{\partial x} + \frac{\partial \tau_{yz}}{\partial y} + \frac{\partial(-p + \tau_{zz})}{\partial z} + S_{Mz} \quad (2.5)$$

The first law of thermodynamics illustrated the energy equation in which the rate of energy change of a fluid element is equivalent to the total of net heat exerted on the fluid element and the net work done on the fluid element which is expressed as follow,

$$\begin{aligned} [-div(\rho u)] + \left[ \frac{\partial(u\tau_{xx})}{\partial x} + \frac{\partial(u\tau_{yx})}{\partial y} + \frac{\partial(u\tau_{zx})}{\partial z} + \frac{\partial(v\tau_{xy})}{\partial x} + \frac{\partial(v\tau_{yy})}{\partial y} + \frac{\partial(v\tau_{zy})}{\partial z} + \right. \\ \left. \frac{\partial(w\tau_{xz})}{\partial x} + \frac{\partial(w\tau_{yz})}{\partial y} + \frac{\partial(w\tau_{zz})}{\partial z} \right] \end{aligned} \quad (2.6)$$

The heat flux generated through heat conduction on the fluid element can be expressed in Equation 2.7,

$$-div q = div(k\nabla T) \quad (2.7)$$

and the specific energy of the fluid element,  $E$  is the sum of kinetic energy and internal energy,

$$E = \frac{1}{2}(u^2 + v^2 + w^2) + i \quad (2.8)$$

By combining the effect of heat conduction, specific energy and potential energy as source term  $S_E$ , the energy equation is expressed as follows,

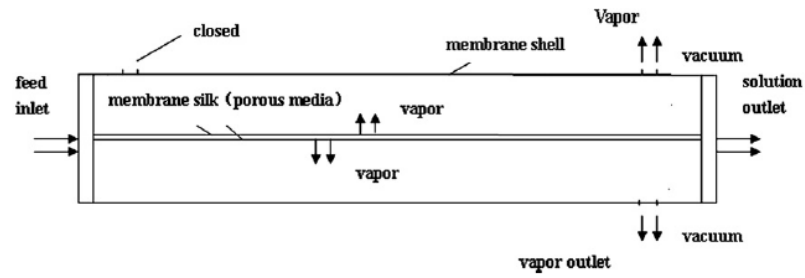
$$\rho \frac{DE}{Dt} = [-div(\rho u)] + \left[ \frac{\partial(u\tau_{xx})}{\partial x} + \frac{\partial(u\tau_{yx})}{\partial y} + \frac{\partial(u\tau_{zx})}{\partial z} + \frac{\partial(v\tau_{xy})}{\partial x} + \frac{\partial(v\tau_{yy})}{\partial y} + \frac{\partial(v\tau_{zy})}{\partial z} + \frac{\partial(w\tau_{xz})}{\partial x} + \frac{\partial(w\tau_{yz})}{\partial y} + \frac{\partial(w\tau_{zz})}{\partial z} \right] + div(k\nabla T) + S_E \quad (2.9)$$

### 2.3.2 Advantages of CFD in DCMD Simulation Study

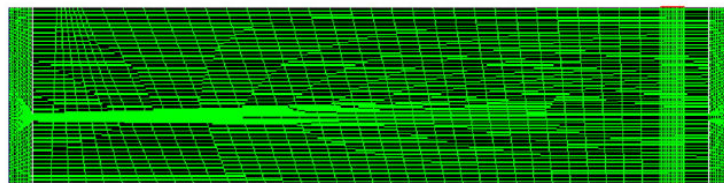
The separation mechanism of DCMD is the vapor pressure differences that drive the vapor transport across the membrane, and hence the major governing factor in this system is the temperature difference. However, the available technology such as non-intrusive techniques like particle image velocimetry (PIV) is unable to obtain the thermal and flow information inside the membrane. Several literature studies have derived the semi-empirical correlation to resolve the heat and mass transfer phenomenon in the DCMD, but it was based on a simplified one dimensional solution (Yu et al., 2011). Hence, the CFD simulation can be adopted in order to obtain a more comprehensive and reliable information on the thermal and flow fields. The CFD modeling is able to comprehensively study and provide a contour of temperature distribution in the membrane module by solving the Navier-Stoke equation coupled with mass and energy equations (Ghidossi et

al., 2006). Subsequently, the result generated from the temperature distribution is able to be extracted to determine thermal efficiency in the DCMD system, and therefore the evaluation of the heat loss through conduction and/or latent heat is possible. As a result, an insight on the heat and mass transfer phenomenon is observed, indicating that the CFD modeling can be performed as a guide to improve the DCMD system performance.

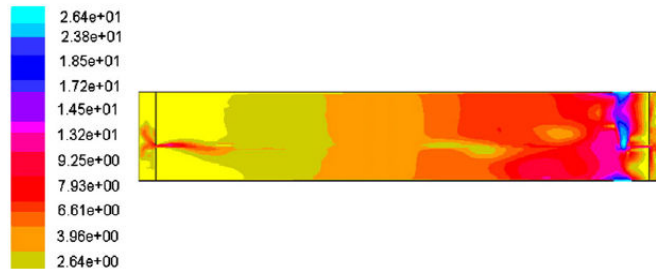
Recently, numerous CFD analyses have been studied in order to numerically simulate the fluid flow mechanism and properties inside the membrane module in several membrane processes. CFD simulation is able to reduce the timeline for the researchers in understanding the hydrodynamics phenomenon involved in the membrane process relative to experimental studies and mathematical approach. Tang et al. (2011) performed the CFD simulation on the permeate flux under the effect of feed flow rate on the NaCl rejection in a VMD system (Figure 2.13). In this study, the membrane module was simplified into a 2D rectangular membrane module in the geometry modeling. The results of the simulation were agreeable with the experimental results in which the mixed velocity distribution in the vertical direction in the VMD was presented in Figure 2.13c.



(a)



(b)



(c)

**Figure 2.13 CFD Simulation Result in VMD (a) Geometry Model of the Membrane Module in VMD (b) Structured Mesh on the Geometry Model (c) Results of Mixed Velocity in VMD (Tang et al., 2011)**

Yu et al. (2012) studied the heat and mass transfer phenomenon in the DCMD system with and without baffles. Their results showed that the simulation results had a close agreement with experimental works with an error less than 5%. The temperature distribution profile and velocity flow field were clearly presented in the simulation results showing the effect of the baffles in the membrane module

(Figure 2.14). Nonetheless, there are only limited studies of MD system using CFD simulation due to the complication of the heat and mass transfer in MD relative to other membrane separation techniques.

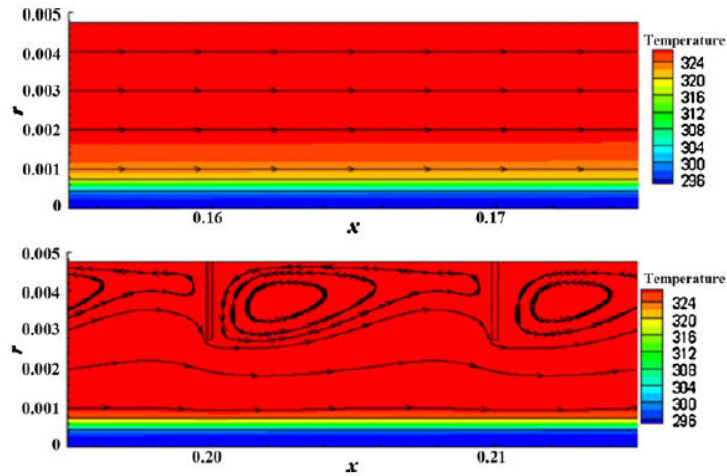


**Figure 2.14 Temperature Distribution and Velocity Flow Field for the DCMD Setup with and without Baffles (Yu et al., 2012)**

## 2.4 Heat Transfer in MD

The heat transfer in the MD system can be basically divided into three stages (Termpiyakul et al., 2005; Qtaishat et al., 2008; Alkhudhiri et al., 2012), i.e., the heat transfer through the feed boundary layer, the heat transfer through the membrane and the heat transfer through the permeate as illustrate in the Figure 2.15. In addition, the heat transfer through the membrane can be further divided into two main components, which are the conduction across the membrane materials and latent heat of vaporization.

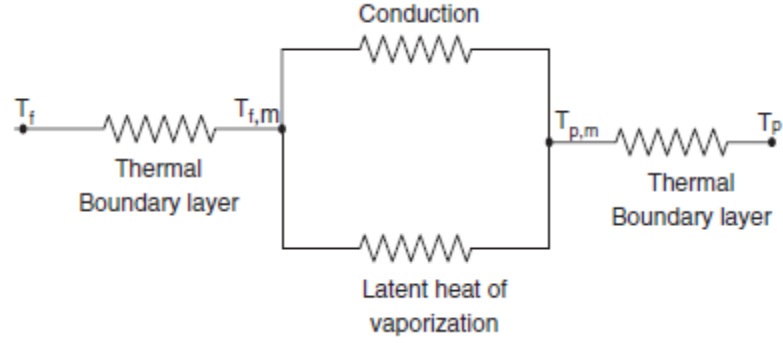


**Figure 2.15 Heat Transfer in DCMD (Alkudhiri et al., 2012)**

As shown in Figure 2.15, the heat transfer at the feed side ( $Q_f$ ) can be expressed in Equation 2.10,

$$Q_f = h_f(T_f - T_{f,m}) \quad (2.10)$$

where  $h_f$  is the heat transfer coefficient of feed solution,  $T_f$  and  $T_{f,m}$  are the feed temperature and feed/membrane interface temperature, respectively.

Furthermore, the heat transfer which involves the movement of the vapor across from the feed side of the membrane to permeate side ( $Q_m$ ) in Equation 2.11 can be expressed as the sum of conduction across the membrane materials,  $Q_c$  and heat transfer by vaporization of liquid,  $Q_v$ ,

$$Q_m = Q_c + Q_v \quad (2.11)$$

The heat conduction across the membrane materials can be determined by Equation 2.12 in which  $h_m$  is the heat transfer coefficient of the membrane, and  $T_{p,m}$  is the permeate/membrane interface temperature (Alkudhiri et al., 2012)

$$Q_c = h_m(T_{f,m} - T_{p,m}) \quad (2.12)$$

In the meantime, heat transfer coefficient is shown in Equation 2.13 where  $k_g$  is thermal conductivity of gas,  $k_m$  is thermal conductivity of membrane material,  $\delta$  is membrane thickness and  $\varepsilon$  is the porosity (Qtaishat et al., 2008).

$$h_m = \frac{k_m \varepsilon + k_p (1 - \varepsilon)}{\delta} \quad (2.13)$$

where thermal conductivity of polymer,  $k_p$  is determined by the isostress model (Phattaranawik et al., 2003) in Equation 2.14,

$$k_p = \left[ \frac{\varepsilon}{k_m} + \frac{(1 - \varepsilon)}{k_g} \right]^{-1} \quad (2.14)$$

In addition, the heat transfer by vaporization of liquid (Khayet and Matsuura, 2011) is expressed in Equation 2.15,

$$Q_v = J\Delta H_{v,w} \quad (2.15)$$

where  $J$  is the transmembrane flux, and  $\Delta H_{v,w}$  is the latent heat of vaporization.

The latent heat of vaporization is expressed by using empirical correlation (Lawson and Llyod, 1997; Phattaranawik et al., 2003; Khayet and Matsuura, 2011) as shown in Equation 2.16,

$$\Delta H_{v,w} = 1.7535T + 2024.3 \quad (2.16)$$

where  $T$  is the feed temperature.

Meanwhile, the convection heat transfer between the membrane and permeate side are expressed as follows,

$$Q_p = h_p(T_{p,m} - T_p) \quad (2.17)$$

where  $h_p$  is the heat transfer coefficient of permeate and  $T_p$  is the permeate temperature.

During the steady state of the system, the overall heat transfer flux across the membrane,  $Q$  can be shown in Equations 2.18 and 2.19,

$$Q = Q_f = Q_m = Q_p \quad (2.18)$$

$$h_f(T_f - T_{f,m}) = h_m(T_{f,m} - T_{p,m}) + J\Delta H_v = h_p(T_{p,m} - T_p) \quad (2.19)$$

In addition, the thermal efficiency ( $\eta$ ) of the DCMD system defining the ratio of heat transfer by vaporization of liquid to the sum heat transfer across the membrane (Equation 2.20) is an important parameter to indicate the heat loss in the DCMD system. It is worthy to note that the heat transfer by vaporization of liquid,  $Q_v$  usually comprises of 40 to 80% of energy consumption in the DCMD system (Khayet and Matsuura 2011), whereas the remaining is the heat loss in the system through conduction,  $Q_c$ .

$$\eta = \frac{Q_v}{Q_v + Q_c} \times 100\% \quad (2.20)$$

## CHAPTER 3

### METHODOLOGY

#### 3.1 Membrane Fabrication

##### 3.1.1 Materials

The hydrophobic PVDF polymer in this study was purchased in pellet form from Arkema Inc., USA (Kynar 740). The solvents utilized were 1-methyl-2-pyrrolidone (NMP, >99.5%) and N,N-dimethylacetamide (DMAC, >99.5%) which were both obtained from Sigma Aldrich. In the meantime, non-solvent additives such as lithium chloride (LiCl) and ethylene glycol (EG) were both obtained from Sigma Aldrich whereas polyethersulfone (PES) were bought from Amoco Chemicals with purity more than 99%. The hydrophobic surface modifying macromolecule (SMM) was synthesized in the lab similar to the literature (Sisakht et al., 2012) utilizing Zonyl BA-LTM (low fraction 2-(perfluoroalkyl) ethanol), methylene bis (p-phenyl isocyanate) (diphenylmethane diisocyanate; MDI) and  $\alpha$ ,  $\omega$ -aminopropyl poly (dimethyl siloxane) (PDMS).

##### 3.1.2 Preparation of Dope Solution

Pre-treatment was needed for the PVDF pellet which was dried at 70 °C for 24 hours in vacuum oven in order to eliminate the moisture. Prior to the

spinning of the HF membrane, the dope solutions were stirred until it became homogenous and was degassed at room temperature for 24 hours. The composition of the spun membranes is listed in Table 3.1. The spun membranes were labeled as PVDF-NMP, PVDF-EG, PVDF-EG-PES, PVDF-SMM, PVDF-DMAC and PVDF-LiCl for ease of reference.

**Table 3.1 Composition of Spun Membrane**

Membrane	PVDF (wt%)	NMP (wt%)	DMAC (wt%)	EG (wt%)	<sup>a</sup> PES (wt%)	SMM (wt%)	LiCl (wt%)
PVDF-NMP	18	82	–	–	–	–	–
PVDF-EG	18	76	–	6	–	–	–
PVDF-EG-PES	18	76	–	6	5	–	–
PVDF-SMM	18	81	–	–	–	1	–
PVDF-DMAC	17	–	83	–	–	–	–
PVDF-LiCl	12	–	83	–	–	–	5

<sup>a</sup>The addition of PES polymer was based on the composition of PVDF in membrane dope solution

### 3.1.3 Spinning of HF Membrane

The HF membranes were fabricated using dry-wet phase inversion technique which has been described elsewhere (Ismail et al., 1999) and the detailed spinning parameters are summarized in Table 3.2. The spun HF membranes were drenched in water bath for removing additives and dried at room temperature for two days before being utilized in the experimental study.

**Table 3.2 Spinning Parameters of HF Membranes**

Parameter	Value/Type
Dope extrusion rate (ml/min)	4.5
Spinneret OD/ID (mm/mm)	1.3/0.6
Bore liquid	Distilled water
Bore liquid temperature (°C)	25
Bore liquid flow rate (ml/min)	2
External coagulant	Tap water
External coagulant temperature (°C)	25
Air gap distance (cm)	10
Room relative humidity (%)	55 ± 5

### 3.2 Membrane Characterization Techniques

#### 3.2.1 Membrane Morphology

Scanning electron microscope (SEM) is an electron microscope which is able to produce high resolution image by scanning the sample through a focus of electron beam. In this study, SEM (S3400N, Hitachi, Japan; Figure 3.1) was utilized to obtain the membrane morphology. The pre-treatment of the HF membrane prior to the SEM analysis was to cryogenically crack the HF membrane in the liquid nitrogen and attach it to the sample holder using carbon tape. Then, the sample was sputtered with a deposit of gold by sputter coater machine (SC 7620, Emitech, United Kingdom) to increase the electronic conductivity of the sample surface. Furthermore, the sample was examined under an accelerated voltage of 10 kV and eventually a few SEM images were captured.

The membrane morphologies in cross-sectional, inner and outer surfaces were extracted from the SEM images. The pore sizes of the HF membrane were measured based on the SEM images and the pore size distribution was drawn using spreadsheet application program.



**Figure 3.1 Scanning Electron Microscope (Hitachi, 2014)**

### **3.2.2 Porosity**

Membrane porosity ( $\epsilon$ ) is an essential parameter which describes the total void volume fraction open of a membrane. In this study, gravitational method was used to determine the membrane porosity (Bourawi et al., 2006). This method first measured the dry weight of the HF membrane, and then the HF membrane was immersed in 2-butanol (Fisher Scientific, >99%) solution for two hours to fill up the membrane pores before being dried at the room temperature. 2-butanol was selected as the wetting agent for the HF membranes due to its ability to adequately wet the hydrophobic membrane and advantage of not swelling the

membrane. The weight of the HF membrane was subsequently re-measured. These steps were repeated three times for every membrane sample to ensure the accuracy. Subsequently, the porosity can be calculated based on the ratio of the volume of membrane pore to the total volume of the membrane sample, as shown in Equation 3.1 and the calculation of membrane porosity can be obtained in Appendix A (Ahmad et al., 2012),

$$\varepsilon = \frac{(W_1 - W_2) / \rho_W}{(W_1 - W_2) / \rho_W + W_2 / \rho_b} \times 100\% \quad (3.1)$$

where  $W_1$  is the weight of the wetted membrane,  $W_2$  is the weight of dry membrane,  $\rho_b$  is the specific gravity of PVDF (1.78 g/cm<sup>3</sup>) whereas  $\rho_W$  is the specific gravity of 2-butanol (0.81 g/cm<sup>3</sup>)

### 3.2.3 Contact angle

Membrane contact angle is a measurement to indicate the hydrophobicity/hydrophilicity of a membrane (Khayet and Matsuura 2011). The measurement method in this study was static sessile drop technique by contact angle goniometer (Ramé-Hart, USA; Figure 3.2). A droplet of distilled water was dripped by automatic injection syringe on ten spots across the membrane surface to yield an average result of contact angle (The sample of contact angle images is shown in Appendix B).



**Figure 3.2 Contact Angle Goniometer (Ramé-Hart Instrument Co., 2013)**

### **3.2.4 Liquid Entry Pressure**

Liquid entry pressure (LEP) also known as wetting pressure is a measurement of maximum transmembrane pressure applied to the membrane prior to the penetration of liquid into membrane pore, leading to wetting. The LEP measurement method was similar to that used by Smolders and Franken (1989) and García-Payo et al. (2010) as shown in Figure 3.3. Five hollow fiber membranes with an effective length of 10 cm were attached to a tube with epoxy resin adhesive and connected to a pressurized water tank filled with distilled water. First, a low pressure of 0.3 bar was applied to the water tank for ten minutes in order to degas the membranes. Subsequently, the pressure was increased in a stepwise rate of 0.1 bar progressively until the first drop of distilled water appeared on the surface of the HF membrane or a continuous flow of permeate was observed. This corresponding pressure applied to the membrane was named as the LEP. The measurement was repeated three times for each self-

fabricated membrane for better accuracy of the measured results (A sample calculation of LEP is illustrated in Appendix C).

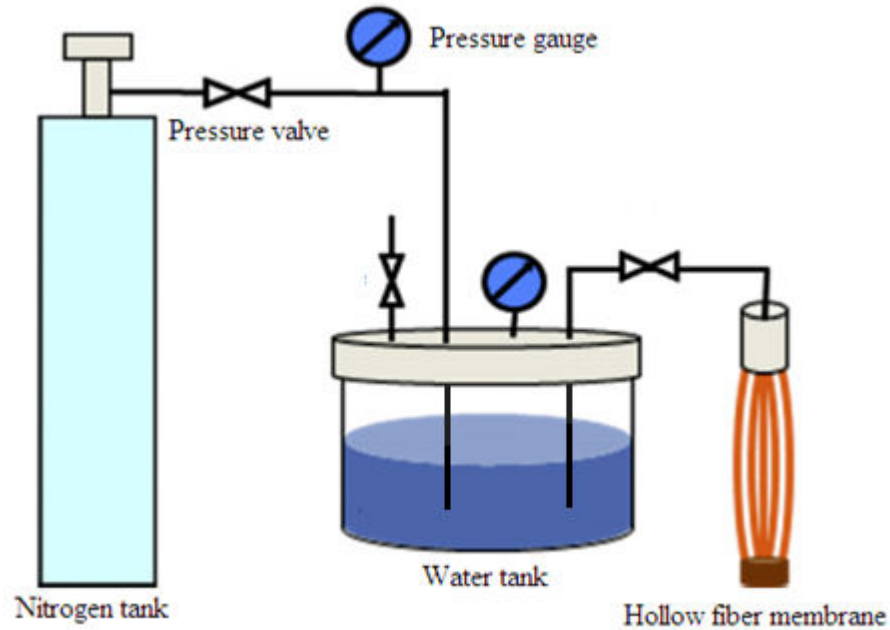


**Figure 3.3 Schematic Diagram of Liquid Entry Pressure Test (García-Payo et al., 2010)**

### 3.3 Experimental Setup

The DCMD experimental study was carried out to investigate the permeate flux of the fabricated HF membrane with different compositions of dope solutions under various feed temperatures with constant permeate temperature, feed and permeate inlet flow rates. Subsequently, the membrane with superior permeate flux was selected to further investigate the performance under different operation parameters such as feed and permeate inlet flow rates. Lastly, a stability test was performed with an extended sampling time up to twenty hours in order to study its performance stability in terms of permeate flux and rejection rate.

Figure 3.4 demonstrates the schematic diagram of DCMD system setup in this study. Sixteen HF membranes with the length of 23 cm and average inner diameter of 450  $\mu\text{m}$  (the effective surface area is 5,204  $\text{mm}^2$ ) were inserted into the membrane module with both ends sealed up with epoxy adhesive. The feed and permeate solution were cross flow in the membrane module in which the feed flew through membrane lumen whereas permeate flowing at the shell side. The feed and permeate solution were re-circulated in close loop within the system by the assist of booster pump. The feed solution consisting of synthesis seawater (3.5 wt% NaCl) was heated to the temperature range of 40 to 55°C using an electrical heating plate (HTS-1003, LMS, Japan). The feed solution was pumped into the lumen side of the HF membrane with booster pump from feed tank with a close loop configuration in the system. In the meantime, permeate solution was cooled down by electrical chiller (CA-1112CE, Eyela, Japan) to a constant temperature of 18°C throughout the whole study. The permeate solution was pumped into the shell side of the membrane module and permeate was collected by condensation of the feed vapor. Both feed and permeate solution flow rates were controlled by a needle valve (SS-1RS4, Swagelok, USA) and flow rate was observed by water flow rotameter (F-550, Blue White, USA) at the range of 0.1 to 0.6 L/min for both feed and permeate inlet. The permeate quality was monitored by an electronic conductivity meter (4520, Jenway, United Kingdom), whereas the weight of the collected permeate was recorded using electronic weight balance (GF6100, A&D, Japan) with data logger (AD1688, A&D, Japan).

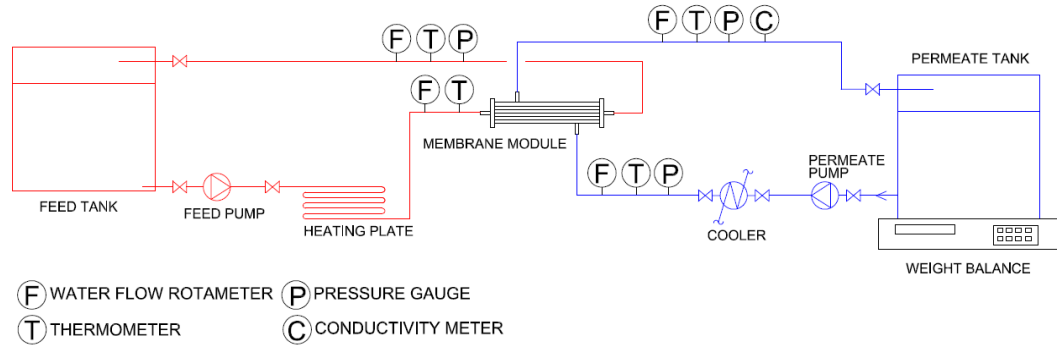


**Figure 3.4 Schematic Diagram of DCMD System Setup**

The permeate flux produced by the membrane,  $J$  (kg/m<sup>2</sup>hr) was determined by Equation 3.2 which has been widely applied in the DCMD literature,

$$J = \frac{\Delta W}{A\Delta t} \quad (3.2)$$

where  $\Delta W$  is the difference between the final and initial permeate weight (kg),  $A$  is the effective surface area of the membrane (m<sup>2</sup>) whereas  $\Delta t$  is the sampling time (h).

Further, the NaCl rejection rate,  $R$  (%) was calculated using Equation 3.3,

$$R = \frac{C_f - C_p}{C_f} \quad (3.3)$$

where  $C_f$  is the feed concentration and  $C_p$  is the permeate concentration.

### 3.4 CFD Simulation

#### 3.4.1 Development of CFD Model

The dimension of the cylindrical membrane housing used in the experimental study had a length of 230 mm and a diameter of 25 mm. However, a simplified two dimensional (2D) geometry model with an assumption of single rectangular HF membrane module in the housing (Figure 3.5) according to the actual dimension was generated for the CFD modeling using Gambit v2.4.6 for the ease of calculation. The geometry model of the membrane module and housing was assumed to be exactly axial symmetric on the  $x$ -direction. Subsequently, the geometry model was meshed with structured quadrilateral elements (Figure 3.6) with different cell sizes (2530, 4605, 10120, 40480, 63250, 253000 and 1012000), generating the resultant meshing structure of the geometry model from coarse to fine mesh size. This trial-and-error meshing size approach was important in following the grid independence analysis of the model in order to obtain an optimum mesh size, while maintaining the acceptable computing time and high accuracy of the simulation results.

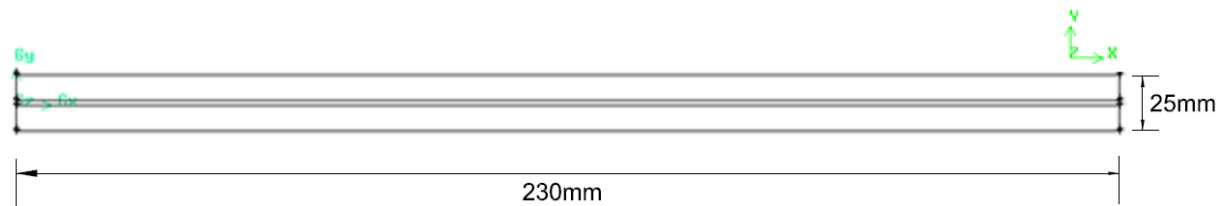


**Figure 3.5 2D Geometry Model of the Membrane Module**

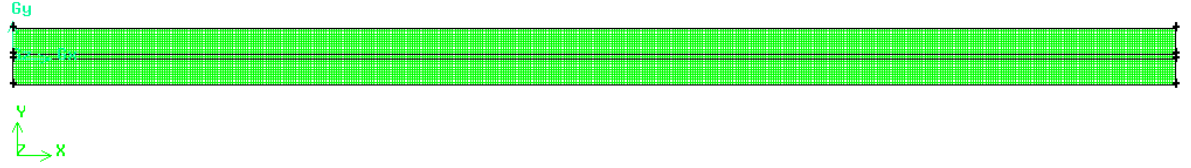


**Figure 3.6 2D Geometry Model with 1:0.5 Mesh Size (10120 cells size)**

The boundary types of the geometry model (Figure 3.7) were identical to the operating parameters in the experimental study. The feed inlet was set as velocity-inlet with a range of 0.1 to 0.7 m/s and fluid temperature ranging 40 to 55 °C. Similarly, the permeate inlet was defined as velocity-inlet with a velocity between 0.01 to 0.02 m/s and a constant temperature of 18 °C. At the other end, both feed and permeate outlets were set as pressure-outlet at gauge pressure (0 Pa). Furthermore, the module casing and membrane were set as wall with no-slip stationary wall condition. Meanwhile, the module wall, membrane material, feed and permeate solution were set to stainless steel, PVDF-EG-PES material, synthetic seawater (3.5 wt% of NaCl) and pure water, respectively. The detailed boundary conditions for the geometry model are listed in Table 3.3.

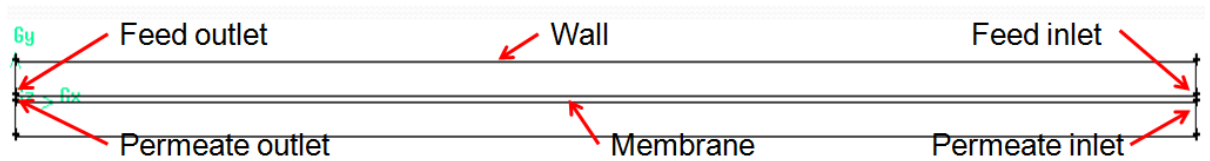


**Figure 3.7 2D Geometry Model with Boundary Type**

**Table 3.3 Boundary Conditions of 2D Geometry Model**

Boundary Condition	Parameter
Feed inlet	Velocity-inlet, 0.1 – 0.7 m/s, 40 – 55 °C
Permeate inlet	Velocity-inlet, 0.01 – 0.02 m/s, 18 °C
Feed outlet	Pressure-outlet, 0 Pa (gauge pressure)
Permeate outlet	Pressure-outlet, 0 Pa (gauge pressure)
Membrane housing	Wall with no slip stationary condition, stainless steel material properties ( $\rho = 8030 \text{ kg/m}^3$ , $c_p = 502.48 \text{ J/kg.k}$ , $k = 16.27 \text{ W/m.K}$ )
Membrane module	Wall, with no slip stationary condition, PVDF-PES material properties ( $\rho = 1780 \text{ kg/m}^3$ , $c_p = 1430 \text{ J/kg.K}$ , $k = 0.0324 \text{ W/m.K}$ )
Synthesized seawater (3.5 wt %)	$\rho = 1025 \text{ kg/m}^3$ , $c_p = 4182 \text{ J/kg.k}$ , $k = 0.6 \text{ W/m.K}$ , $\mu = 0.001003 \text{ kg/m.s}$
Pure water	$\rho = 998.2 \text{ kg/m}^3$ , $c_p = 4182 \text{ J/kg.k}$ , $k = 0.6 \text{ W/m.K}$ , $\mu = 0.001003 \text{ kg/m.s}$

The simulation was performed using a commercial CFD software, namely ANSYS Fluent 6.3 with a two dimensional model to study the heat and mass transfer phenomenon in the previously described geometry model. The pressure based solver which is applicable to wide flow regime with less memory space requirement was adopted in this study using SIMPLE (semi-implicit method for pressure linked equation). The scheme for the discretization of the mass, momentum and energy equation was conducted by second-order upwind technique which provides a higher precision with second order accuracy. The absolute convergence criterion in this study was  $10^{-4}$  for the residual of mass,

momentum and continuity equation, whereas  $10^{-6}$  for residual of energy equation to be converged.

### **3.4.2 Grid Independence Analysis**

In order to study the grid independence of the model, the geometry model was meshed to different cell sizes as seen in Table 3.4 which varying from coarse to fine mesh (Versteeg and Malalasekera, 1995).

In this analysis, the parameters applied in the experimental study for both feed and permeate inlets were defined in the boundary condition, whereas feed outlet velocities as a criterion in comparison were numerically calculated and compared with experimental value of 0.39 m/s under the experimental conditions of feed inlet mass flow rate and temperature of 0.3 L/min and 55 °C, respectively and permeate inlet mass flow rate of 0.3 L/min and 18 °C, respectively to determine the optimum mesh size. The grid independence results are tabulated in Table 3.4. It was clearly observed that there was negligible difference from mesh size of 63,250 and onwards (relative error <1%), concluding that this mesh size was sufficient for this geometry model.

**Table 3.4 Grid Independence Analysis Based on Feed Outlet Velocity (m/s)**

---

No. of cell	Experimental value	CFD value	Relative error (%)
2,530	0.39	0.40829817	4.69
4,605	0.39	0.40229799	3.15
10,120	0.39	0.39629790	1.61
40,480	0.39	0.39429787	1.10
63,250	0.39	0.39229754	0.59
253,000	0.39	0.39229721	0.58
1,012,000	0.39	0.39219712	0.56

---

## CHAPTER 4

### RESULTS AND DISCUSSION

#### 4.1 DCMD Experimental Study

##### 4.1.1 Membrane Characteristics

###### 4.1.1.1 Membrane Morphology

The SEM images on the morphology of PVDF HF membrane prepared with and without additive are show in Figures 4.1 – 4.6. The structure of the PVDF-NMP membrane (Figure 4.1) showed a finger-like layer extending from the inner layer to outer surface. The formation of this membrane structure was attributed to the nature of NMP as a strong solvent in the water solution (non-solvent) during the dry/wet phase inversion process. The interaction between NMP and water coagulation bath triggered the rapid diffusion of NMP and the formation of surface layer. In a short while, the diffusion rate of NMP slowed down which encouraged the growth of membrane pores and led to the formation of finger-like layer (Young and Chen, 1995).

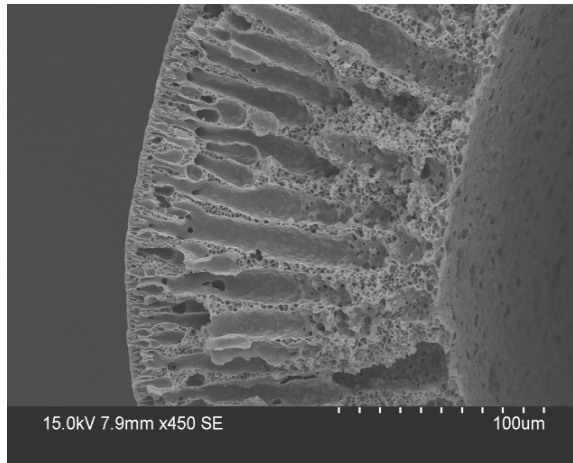


**Figure 4.1** Cross Sectional SEM Image of PVDF-NMP

The structure of PVDF-EG (Figure 4.2) illustrated a decreased finger-like structure on the inner and outer surfaces with an intermediate layer of irregular microvoids. The formation of the microvoids was due to the increase of viscosity in membrane dope solution as a result of the addition of EG (Liao et al., 2013). The higher viscosity dope solution of PVDF-EG (viscosity at 2886 cP) relative to (viscosity at 2367 cP) led to the decrease of water intrusion to the middle layer of HF membrane which allowed the formation of microvoids.



**Figure 4.2** Cross Sectional SEM Image of PVDF-EG

Figure 4.3 presents the membrane structure of PVDF-EG-PES which demonstrated a finger-like layer extending from inner layer and outer surface separated by a thin sponge-like structure. The formation of this structure might suggest the thermodynamically incompatible system of PVDF and PES due to the difference in the solubility of  $15.1 \text{ (cal/cm}^2)^{1/2}$  and  $11.19 \text{ (cal/cm}^2)^{1/2}$  respectively (Wu et al., 2006). The finger-like layer grew from the inner layer to outer due to the rapid diffusion of NMP into coagulation bath. However, the growth rate of the finger-like layer was delayed as large volume of PES dispersing in the solution which led to the growth of sponge-layer at the intermediate layer as a result of delay of demixing.

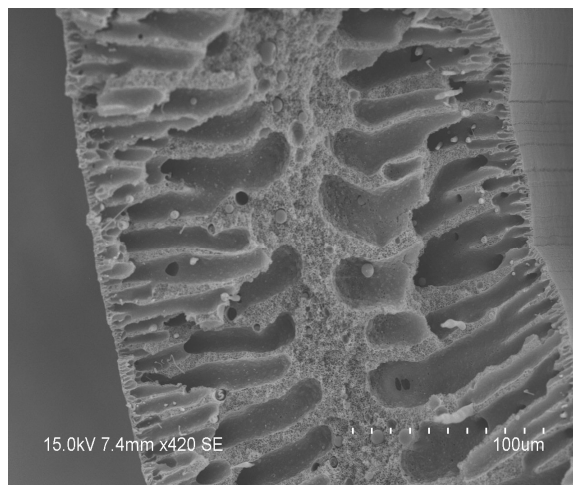


**Figure 4.3 Cross Sectional SEM Image of PVDF-EG-PES**

When SMM was added into the dope solution, the PVDF-SMM membrane structure (Figure 4.4) displayed a finger-like microvoids layer developed from inner and outer layer to the center thin sponge-like layer. (Sisakht

et al., 2012). The microvoids structure formation might suggest a rapid phase inversion between polymer solution with the strong coagulation bath (Yuliwati et al., 2011).

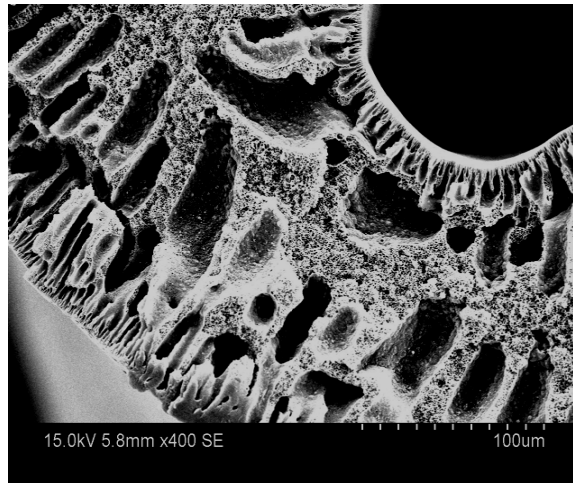


**Figure 4.4** Cross Sectional SEM Image of PVDF-SMM

In addition, the PVDF-DMAC membrane (Figure 4.5) displayed a similar membrane structure as PVDF-NMP in which a finger-like layer developed from the inner membrane layer to the outer membrane layer. Identical to NMP, DMAC exhibited the strong solvent characteristic as well when interacting with the non-solvent solution, leading to the early occurrence of liquid-liquid phase separation during the induced phase inversion due to the rapid diffusion of DMAC (Yeow et al., 2004).

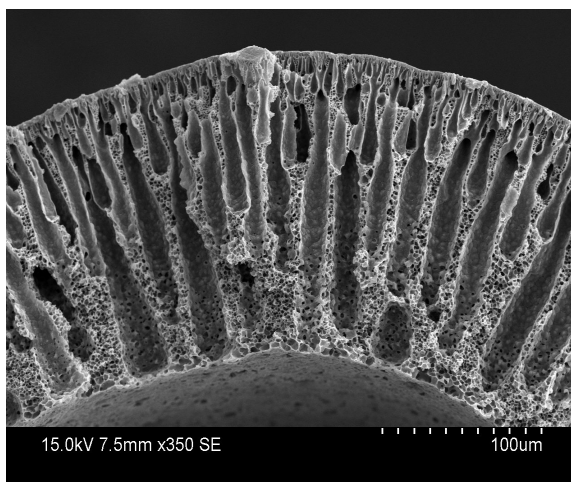


**Figure 4.5** Cross Sectional SEM Image of PVDF-DMAC

The PVDF-LiCl membrane as presented in Figure 4.6 exhibited a membrane structure of sponge-like layer with microvoids. This microvoid formation was probably attributed to the increment of the PVDF precipitation rate during the membrane immersion in the coagulation bath as a result of LiCl additive (Bottino et al., 1988).

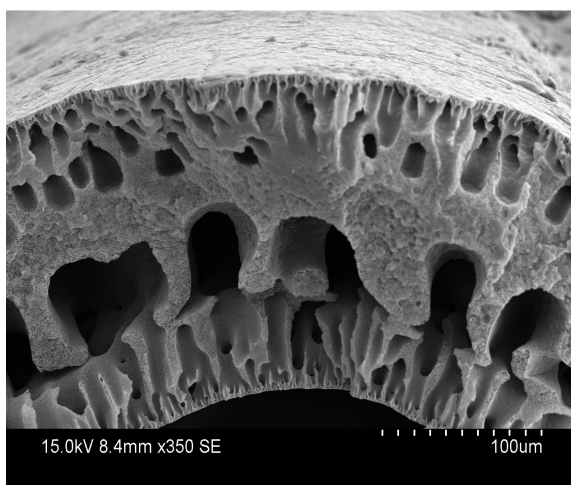


**Figure 4.6** Cross Sectional SEM Image of PVDF-LiCl

#### 4.1.1.2 Membrane Thickness

The thickness of the self-fabricated membranes was measured to be in the range of 180 to 280  $\mu\text{m}$  (Table 4.1) which is similar to the range (130 to 330  $\mu\text{m}$ ) of membrane thickness as reported in literature (Hou et al., 2009, Mansourizadeh, and Ismail, 2010, Sisakht et al., 2012). It was worth noting that PVDF-EG-PES exhibited the thinnest membrane with a thickness of 180  $\mu\text{m}$ , whereas PVDF-NMP had the largest thickness of 280  $\mu\text{m}$ . The thickness of the membrane had an inversely proportional relation to the permeate flux production as a result a better thermal conductivity and mass transfer (Bourawi et al., 2006). Hence, the thinnest membrane thickness of PVDF-EG-PES might contribute to a higher permeate flux relative to other self-fabricated membranes.

**Table 4.1 Self-fabricated Membrane Thickness**

Membrane	Thickness ( $\mu\text{m}$ )
PVDF-NMP	280
PVDF-EG	200
PVDF-EG-PES	180
PVDF-SMM	250
PVDF-DMAC	200
PVDF-LiCl	200

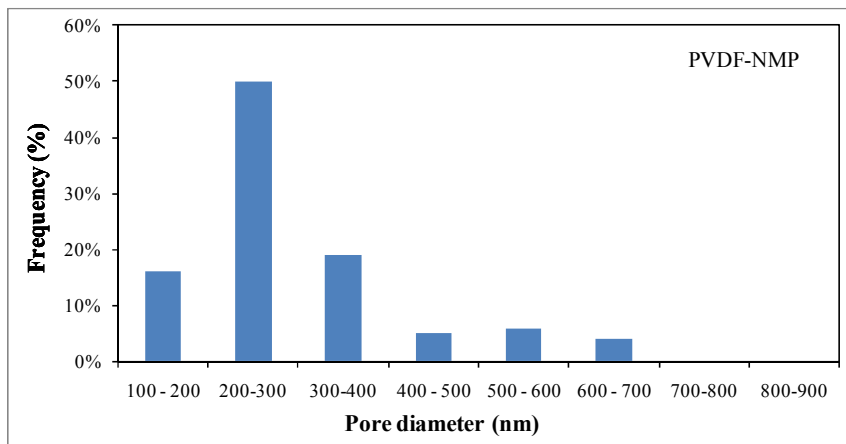
#### 4.1.1.3 Membrane Porosity and Pore Size Distribution

In the meantime, the results from the gravitational method calculation (Table 4.2) revealed that the self-fabricated membrane had a porosity range of 60 – 85% which was fulfilled the porosity requirement (30 to 85%) in MD process as

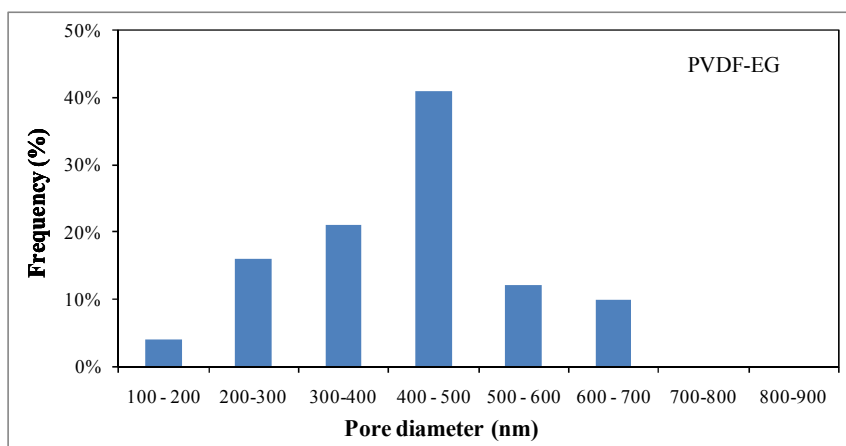
reported by Bourawi et al. (2006). The PVDF-LiCl membrane possesses a highest porosity (85%) compared to other membranes and this was probably attributed to LiCl additive as a pore forming agent (Bottino et al., 1988). However, the major drawback of LiCl additive in the membrane fabrication was the reduction in mechanical strength due to the high porous structure of the membrane which would attribute to the breakage and leakage of the membrane under prolonged operation period (Khayet and Matsuura, 2011). The mean pore sizes for the fabricated membranes in this study were varying between 250 and 450 nm which was comparable to the mean pore size (100 to 510 nm) reported by Alkudhiri et al. (2012). The membrane mean pore size with a descending order was PVDF-EG > PVDF-DMAC and PVDF-LiCl > PVDF-EG-PES > PVDF-SMM > PVDF-NMP (Table 4.2). In addition, the pore size distribution of the membrane as illustrated in Figure 4.7 showed that PVDF-EG-PES had a narrowest pore size distribution which might lead to the consistent rejection rate and minimize water leakage through the membrane.

**Table 4.2 Self-fabricated Membrane Porosity and Mean Pore Size**

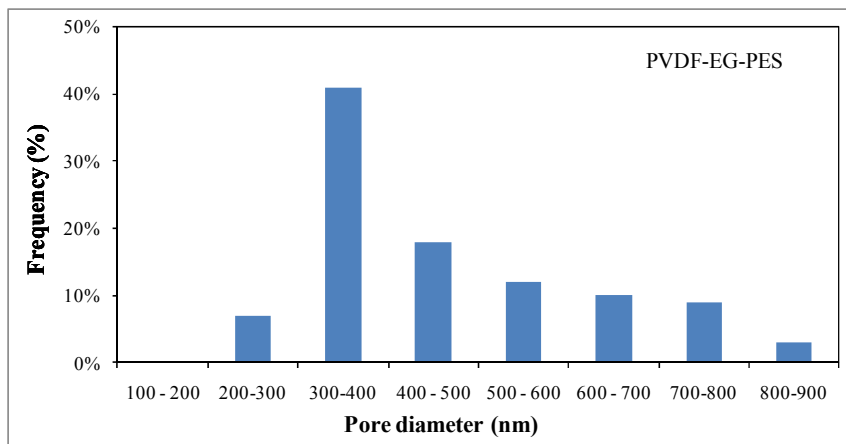
Membrane	Porosity (%)	Mean Pore Size (nm)
PVDF-NMP	80 ± 1.25	250
PVDF-EG	60 ± 2.25	450
PVDF-EG-PES	70 ± 0.75	350
PVDF-SMM	83 ± 0.75	300
PVDF-DMAC	70 ± 0.75	400
PVDF-LiCl	85 ± 1.25	400



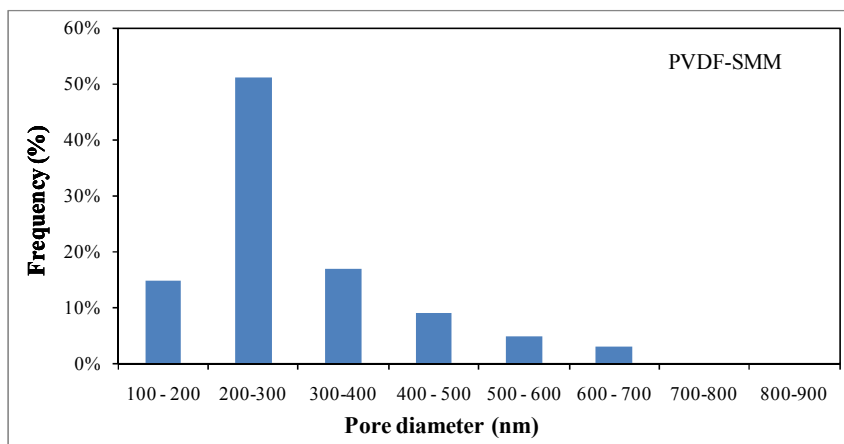
(a)



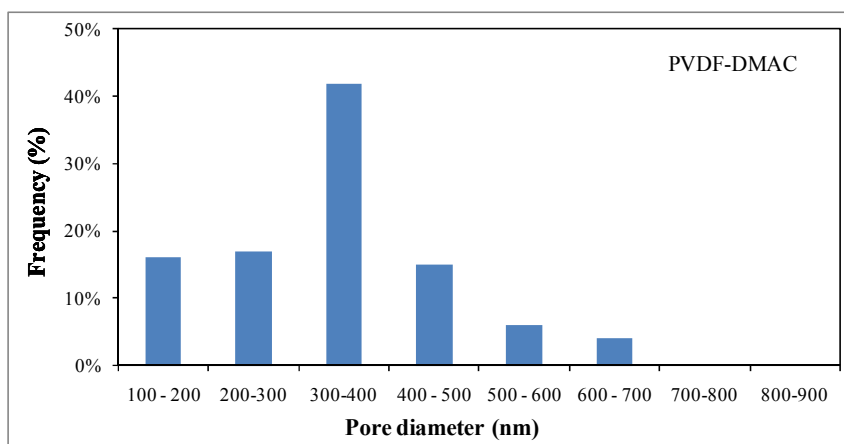
(b)



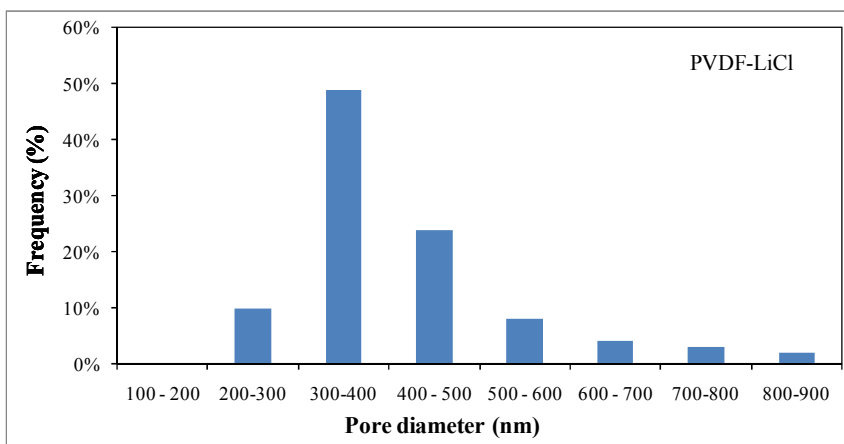
(c)



(d)



(e)



(f)

**Figure 4.7 Pore Size Distributions for (a) PVDF-NMP (b) PVDF-EG (c) PVDF-EG-PES (d) PVDF-SMM (e) PVDF-DMAC (f) PVDF-LiCl**

#### 4.1.1.4 Membrane Contact Angle

A good MD membrane shall exhibit a hydrophobicity characteristic to avoid wetting under long-term operation and this characteristic can be illustrated by contact angle. The membrane contact angles of self-fabricated membranes are presented in Table 4.3. PVDF-SMM possessed the highest contact angle at 92° compared to other self-fabricated membrane. This finding could be attributed to the surface modification by the hydrophobic SMM additive, leading to the higher hydrophobicity. The results from the contact angle study concluded that all the self-fabricated membranes in this study were hydrophobic membranes in which their contact angles were more than 70° as widely discussed in literature (Khayet and Matsuura, 2011).

**Table 4.3 Self-fabricated Membrane Contact Angle**

Membrane	Contact angle (°)
PVDF-NMP	88 ± 0.60
PVDF-EG	82 ± 5.60
PVDF-EG-PES	85 ± 0.20
PVDF-SMM	92 ± 1.25
PVDF-DMAC	76 ± 0.50
PVDF-LiCl	76 ± 0.20

#### 4.1.1.5 Membrane Liquid Entry Pressure

The membrane liquid entry pressure is an important characteristic in the membrane defining its maximum allowable exerted pressure to the membrane before the pore is penetrated by feed liquid or wetted. The liquid entry pressure

for the fabricated membranes is summarized in Table 4.4. The PVDF-EG-PES membrane demonstrated the highest liquid entry pressure relative to other fabricated membrane at 4.0 bar resulting higher resistance to pore wetting (Bourawi et al., 2006) whereas PVDF-DMAC posses the lowest liquid entry pressure at 2.6 bar.

**Table 4.4 Self-fabricated Membrane Liquid Entry Pressure**

Membrane	Liquid entry pressure (bar)
PVDF-NMP	3.50
PVDF-EG	3.70
PVDF-EG-PES	4.00
PVDF-SMM	3.00
PVDF-DMAC	2.60
PVDF-LiCl	2.80

#### 4.1.2 Effect of Temperature on DCMD Performance

Figure 4.8 demonstrates the effect of the various feed inlet temperatures on the permeate flux of self-fabricated membrane under the constant feed inlet flow rate of 0.3 L/min, permeate inlet flow rate and temperature of 0.3 L/min and 18 °C, respectively. The feed inlet temperature exhibited a positive effect on the permeate flux in which the higher the temperature, the higher the permeate flux from feed inlet temperature of 40 to 50 °C. This effect was attributed to the increase of transmembrane thermal vapor pressure as the result of higher temperature difference between the feed and permeate solutions (Khayet and Matsuura, 2011). As displayed in Figure 4.8, it was found that PVDF-EG-PES

yielded the highest permeate flux, possibly due to its thinnest membrane thickness, in addition to good characteristics of porosity and contact angle (Khayet, 2011). As for the PVDF-SMM membrane, the alteration of membrane structure by SMM additive had greatly increased the permeate flux compared to the neat PVDF-NMP membrane. This might be attributed to the increment of membrane contact angle resulting in a greater hydrophobicity to prevent membrane pore wetting and fine characteristic in porosity (Khayet, 2011). Nevertheless, the lowest permeate flux was recorded for the PVDF-DMAC membrane. Its low contact angle would result in membrane pore wetting. In view of the finding that the PVDF-EG-PES membrane possessed the highest permeates flux, it was chosen to be further investigate under different operating parameters in the following sections.

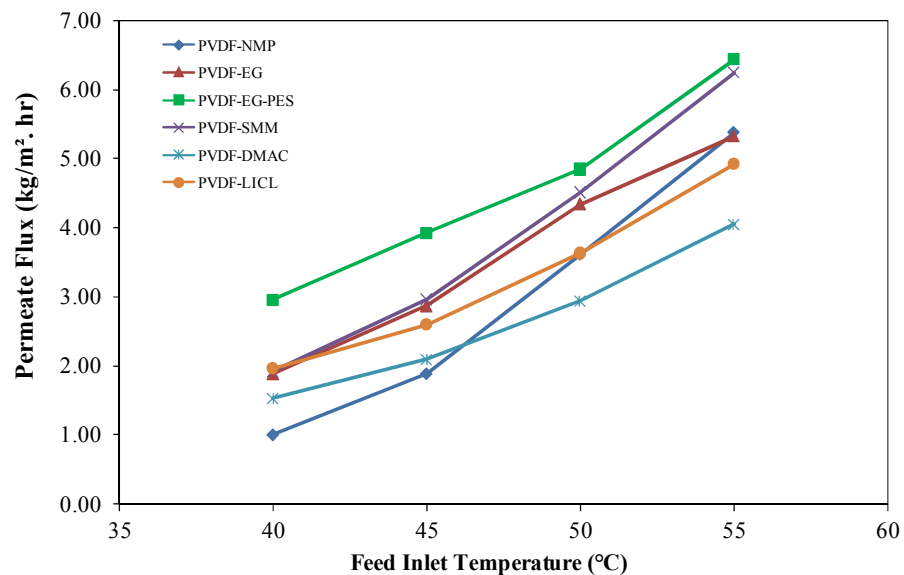


**Figure 4.8 Membrane Permeate Flux as a Function of Feed Inlet Temperature with the Operation Condition of Feed Inlet Flow Rate = 0.3 L/min, Permeate Inlet Flow Rate = 0.3 L/min and Permeate Inlet Temperature = 18 °C**

### 4.1.3 Effect of Flow Rate on DCMD Performance

The effect of two important operation parameters in DCMD, i.e., permeate and feed flow rates on permeate flux were discussed in this section using the PVDF-EG-PES membrane. The green square in Figure 4.9 was the highest permeate flux achieved by the PVDF-EG-PES membrane in the earlier study on temperature effect. Figure 4.9 shows that the permeate flux of the PVDF-EG-PES membrane was strongly dependent on the feed inlet flow rate in which the permeate flux increased with the increment of the feed inlet flow rate. More specifically, the permeate flux increased from 2.92 to 9.23 kg/m<sup>2</sup>.hr or three folds with the increasing feed inlet flow rate from 0.1 to 0.6 L/min. Subsequently, the highest permeate flux (red square in Figure 4.9) was selected to investigate the effect of permeate inlet flow rate on permeate flux.

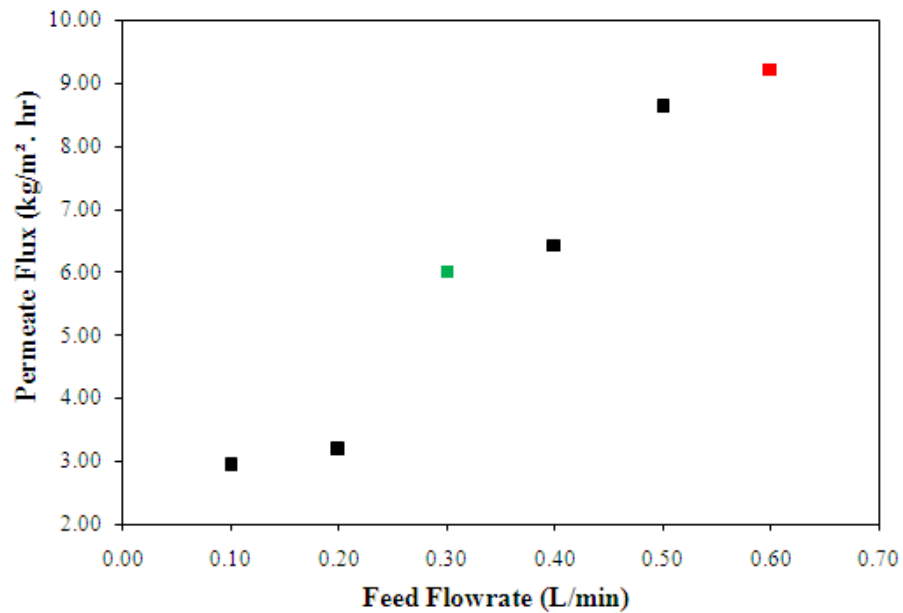


**Figure 4.9 Membrane Permeate Flux as a Function of Feed Inlet Flow Rate with the Operation Condition of Feed Inlet Temperature = 55 °C, Permeate Inlet Flow Rate = 0.3 L/min and Permeate Inlet Temperature = 18 °C**

Identical to Figure 4.9, the similar trend was observed in Figure 4.10 in which the permeate inlet flow rate had a positive effect on the permeate flux (Bahmanyar et al., 2012; Alkhudhiri et al., 2013). The permeate flux increased from 7.88 to 14.12 kg/m<sup>2</sup>.hr or more than 1.5 folds when the permeate flow rate increased from 0.1 to 0.6 L/min. Compared to the permeate inlet flow rate of 0.3 L/min (Figure 4.9), the permeate flux of PVDF-EG-PES was improved approximately 50% from 9.23 to 14.12 kg/m<sup>2</sup>.hr, when the permeate inlet flow rate was controlled at 0.6 L/min.

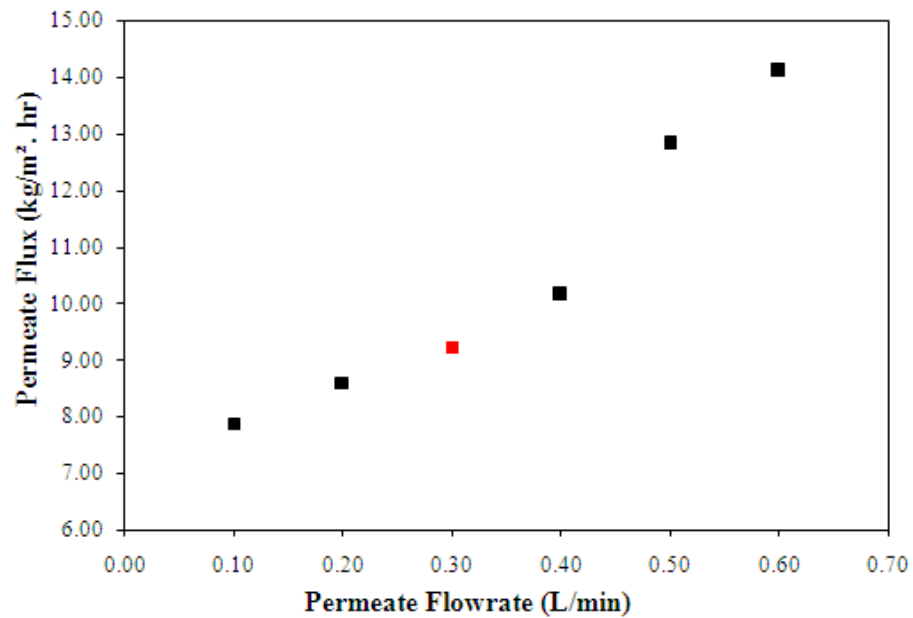


**Figure 4.10 Membrane Permeate Flux as a Function of Permeate Inlet Flow Rate with the Operation Condition of Feed Inlet Temperature = 55 °C, Feed Inlet Flow Rate = 0.6 L/min and Permeate Inlet Temperature = 18 °C**

The effects of permeate and feed flow rates on the permeate flux of PVDF-EG-PES membrane were related to the increase of heat and mass transfer rates across the membrane as a result of the increase of heat transfer coefficient on the feed side as well as the reduction of temperature polarization (Bahmanyar et

al., 2012; Alkhudhiri et al., 2013). However, it is worth mentioning that a high flow rate can result in an elevation of transmembrane pressure. If the transmembrane pressure exceeds the membrane liquid entry pressure, the permeate quality will be deteriorated followed by reduction in permeate flux production on the permeate side due to the increase of pressure polarization (Bahmanyar et al., 2012; Alkhudhiri et al., 2013). Hence, the pressure exerted to the membrane shall be lower than the membrane LEP in determining an optimum flow rate.

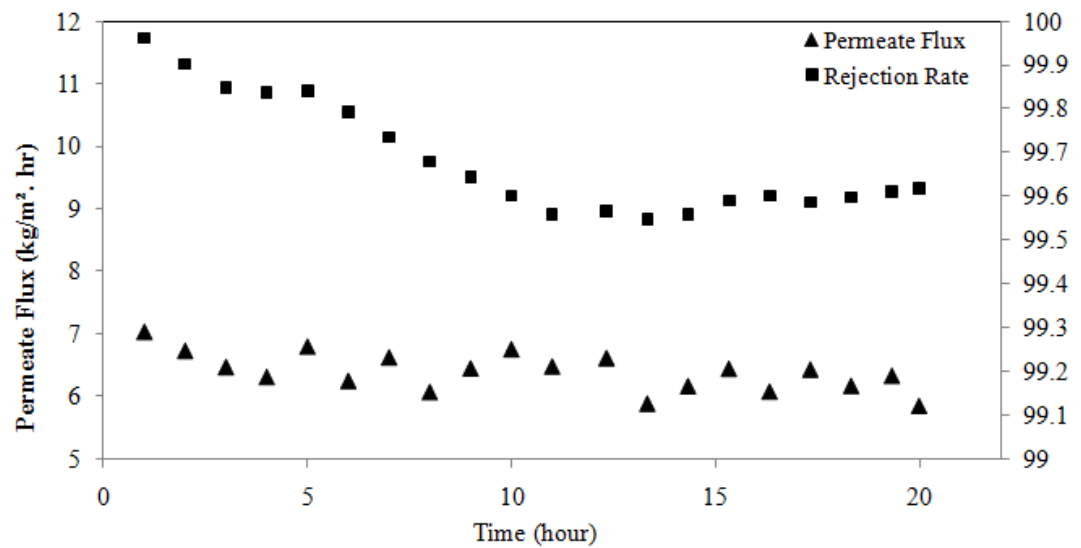
#### **4.1.4 Membrane Stability Test**

The membrane stability test was carried out to evaluate the permeate flux and NaCl rejection rate of PVDF-EG-PES membrane as a function of operating time up to 20 hours. The stability test was carried out with constant feed and permeate inlet temperatures of 55 °C and 18 °C, respectively, while varying both feed and permeate inlet feed flow rates at 0.3 and 0.6 L/min while other operating parameter conditions were similar to the study on in Section 4.1.3.

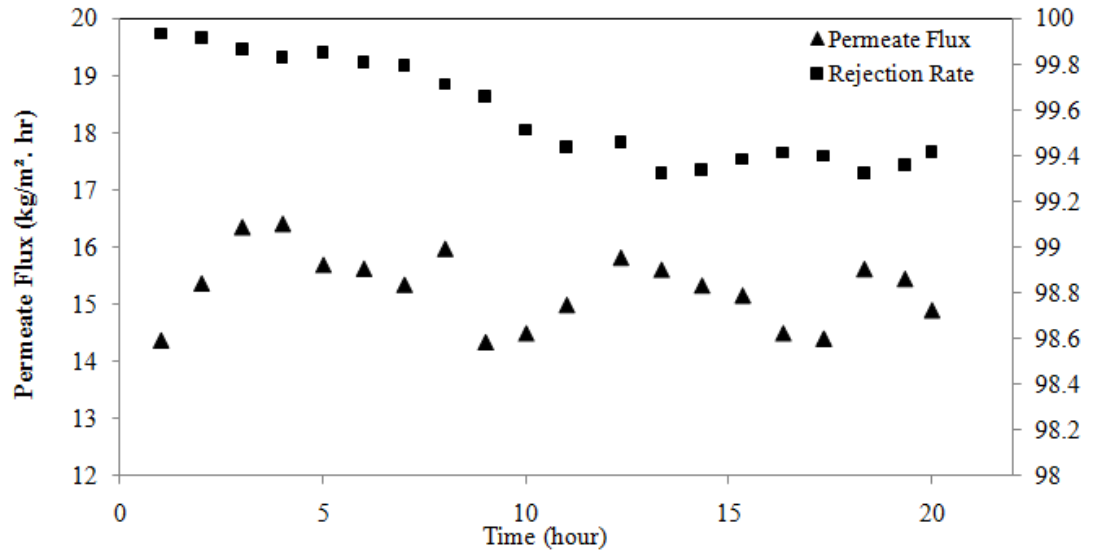
As observed from Figures 4.11 (a) and (b) respectively, the mean permeate flux of the membrane tested at feed and permeate inlet flow rate of 0.3 L/min was 6.4 kg/m<sup>2</sup>.hr, compared to the 15.3 kg/m<sup>2</sup>.hr from the membrane tested at feed and permeate inlet flow rate of 0.6 L/min, respectively. The increase of approximately two folds of the permeate flux was similar to the previous section (Section 4.1.3) in which the enhancement of rate of the heat and mass transfer

across the membrane. Furthermore, it could be observed that the performance stability of the membrane was well maintained in both cases ( $6.4 \pm 0.55 \text{ kg/m}^2 \cdot \text{hr}$  for case (a) and  $15.3 \pm 1.5 \text{ kg/m}^2 \cdot \text{hr}$  for case (b)) in which no significant reduction in permeate flux was discovered.

In the aspect of rejection rate, a slight decrease of rejection rate was observed for both cases with respect to the operating time. The rejection decreased from 99.9% to approximately 99.3% at the end of the studies. The decrease of the rejection rate throughout the operating time was considered as insignificant ( $<0.6\%$ ) which indicated that the membrane had a stable rejection rate (Hou et al., 2009). These stability tests clearly implied that the self-fabricated membranes were suitable for DCMD application in producing fresh water.



(a)



(b)

**Figure 4.11 Membrane Stability Test Under Feed Inlet Temperature (55°C) and Permeate Inlet Temperature (18°C) at Different Stream Flow Rates (a) Feed and Permeate Inlet Flow Rate at 0.3 L/min Respectively (b) Feed and Permeate Inlet Flow Rate at 0.6 L/min Respectively**

#### 4.1.5 Analysis of Thermal Efficiency

Thermal efficiency of the DCMD system is defined by the ratio of latent heat of the water vapor to total heat across the membrane (the total of latent and conduction heat). It should be highlighted the thermal efficiency analysis is able to evaluate how effective the heat is utilized in the system and the strategy to improve the system efficiency in order to conserve the energy used. In this analysis, the PVDF-EG-PES was used as the membrane material. Figure 4.12 presents the effect of temperature of feed inlet on the thermal efficiency of the DCMD system. The thermal efficiency was observed to slightly increase from 54% to 57% with the increment of feed inlet temperature from 40 to 55 °C. This

minor increase in thermal efficiency might be attributed to the heat loss in the system is through conduction.

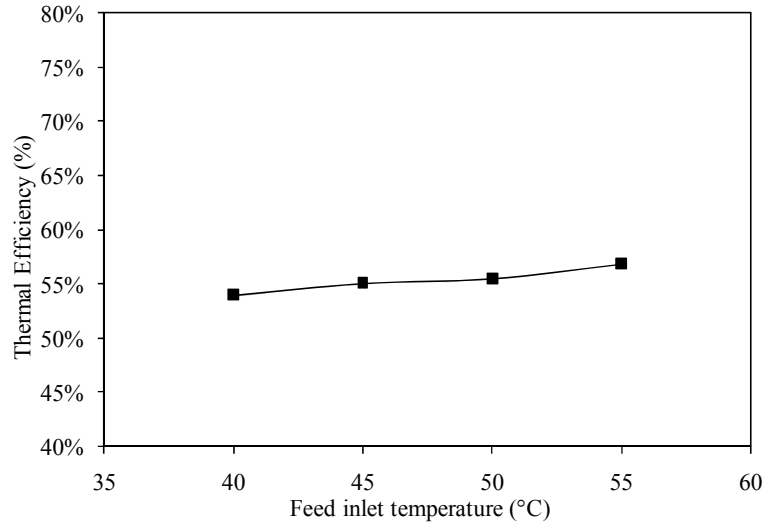


**Figure 4.12 Thermal Efficiency with a Function of Feed Inlet Temperature**

On the other hand, when the feed inlet temperature was remained constant at 55 °C, and the feed and permeates inlet flow rates were adjusted as shown in Figures 4.13 and 4.14 respectively, the thermal efficiency increased drastically. With the increment of feed inlet flow rate from 0.3 to 0.6 L/min under the feed inlet temperature of 55 °C and permeate inlet flow rate of 0.3 L/min, the thermal efficiency increased by 10% from 57% to 67%. In addition, by varying permeate inlet flow rate from 0.3 to 0.6 L/min under the feed inlet temperature of 55 °C and feed inlet flow rate of 0.6 L/min, the thermal efficiency of the DCMD system increased from 67% to 76%. The increment of the thermal efficiency by raising both feed and permeate inlet flow rates could be explained by the elevation of permeate flux which increased the heat transfer by vaporization of liquid ( $Q_v$ )

against the heat conduction across the membrane ( $Q_c$ ) in the system as expressed in Equation 2.15 and 2.20 respectively.

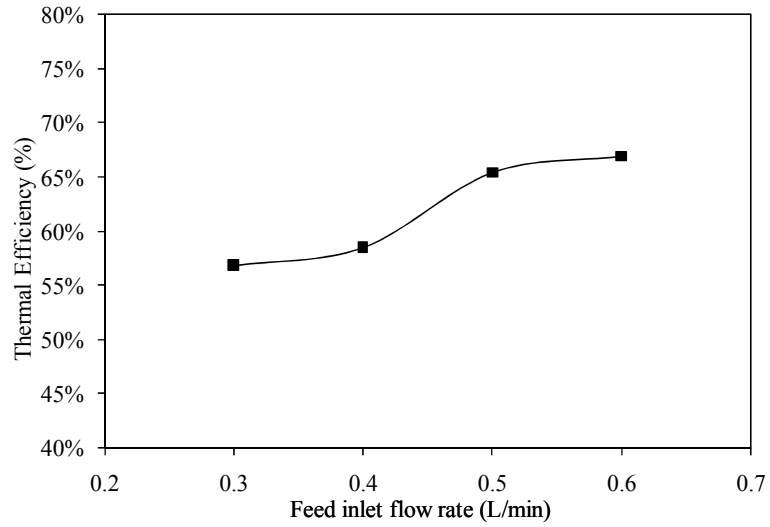


**Figure 4.13 Thermal Efficiency with a Function of Feed Inlet Flow Rate**

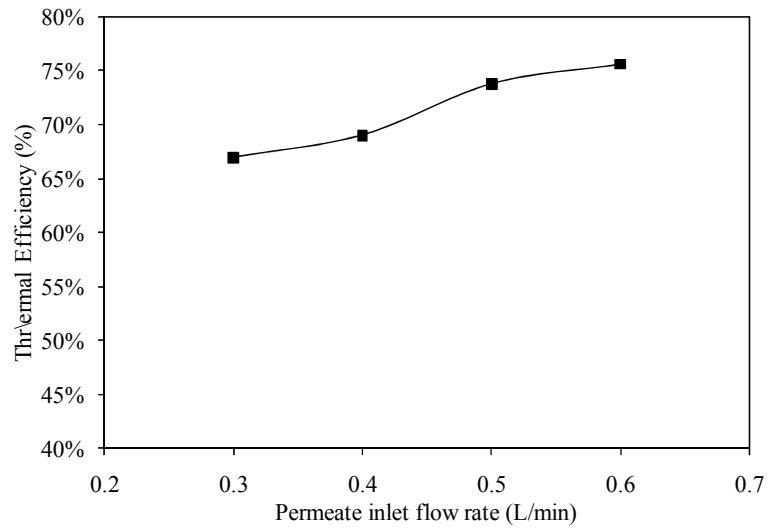


**Figure 4.14 Thermal Efficiency with a Function of Permeate Inlet Flow Rate**

## **4.2 CFD Simulation Study**

### **4.2.1 Temperature Distribution Analysis**

To date, there are no techniques applied practically to capture/analyze the temperature distribution in the membrane module. However, in the CFD simulation, the temperature distribution can be illustrated by the contour of static temperature which allows the user to study the heat transfer phenomenon in the membrane module.

Tables 4.5 and 4.6 tabulate the comparisons between experimental and numerical simulation results in terms of feed and permeate outlet temperatures, respectively. Both of the experimental feed and permeate outlet temperatures were measured with digital thermometers, whereas the CFD feed and permeate outlet temperatures were averaged based on the simulated outlet temperatures of the membrane. As it could be seen in Tables 4.5 and 4.6, the simulation results on both feed and permeate outlet temperatures were found to well agree with the experimental results. The tabulated results showed that the relative deviation for comparison between experimental and CFD simulation for both feed and permeate outlet temperature were in the range of 2.00 to 7.23 % and 1.07 to 4.43 % respectively. These low relative deviations implied that the reliability of the geometry model used in the simulation studies.

**Table 4.5 The Feed Outlet Temperature Comparison between Experimental and CFD Simulation Studies (Feed and Permeate Inlet Flow Rate each at 0.3 L/min)**

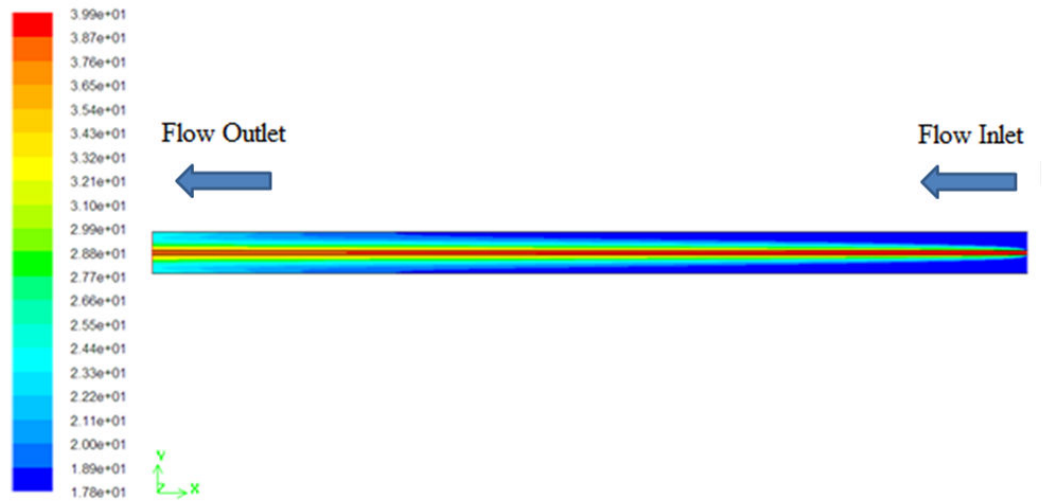
Feed inlet temperature (°C)	Permeate inlet temperature (°C)	Experimental feed outlet temperature (°C)	CFD feed outlet temperature (°C)	Relative deviation (%)
40	18	35.60	38.18	-7.23
45	18	41.80	42.75	-2.27
50	18	46.40	47.33	-2.00
55	18	50.30	51.91	-3.20

**Table 4.6 The Permeate Outlet Temperature Comparison between Experimental and CFD Simulation Studies (Feed and Permeate Inlet Flow Rate each at 0.3 L/min)**

Feed inlet temperature (°C)	Permeate inlet temperature (°C)	Experimental permeate outlet temperature (°C)	CFD permeate outlet temperature (°C)	Relative deviation (%)
40	18	23.30	22.36	4.03
45	18	23.40	23.15	1.07
50	18	23.60	23.93	-1.38
55	18	23.70	24.75	-4.43

Figure 4.15 presents the contour of temperature distribution generated by CFD simulation in the 230 mm long membrane module for the DCMD process under operating conditions of feed inlet temperature varying from 40 to 55 °C, permeate inlet temperature at 18 °C, feed and permeate inlet flow rate each at 0.3 L/min. The results illustrated the hot feed flew within the membrane at the center

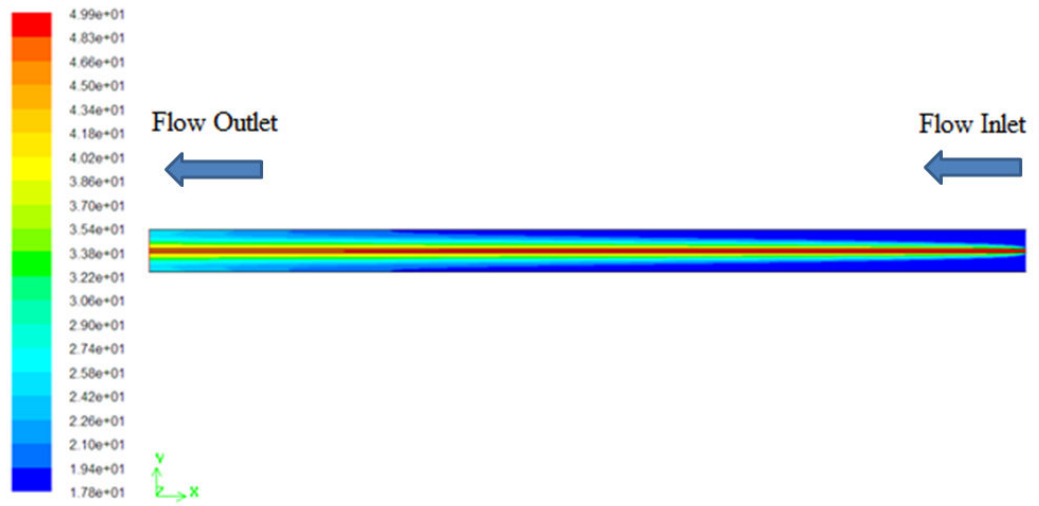
of membrane module, reaching the outlet with a lower temperature relative to the initial temperature at the module entrance. Similarly, the cold permeate flew from the inlet with an initial temperature of 18 °C. The temperatures of the cold permeate increased *x*- and *y*- directions as a result of heat transfer from the hot feed until the end of the membrane module. This trend of temperature distribution contour was consistently observed for all the cases with feed inlet temperature varying from 40 to 55 °C.



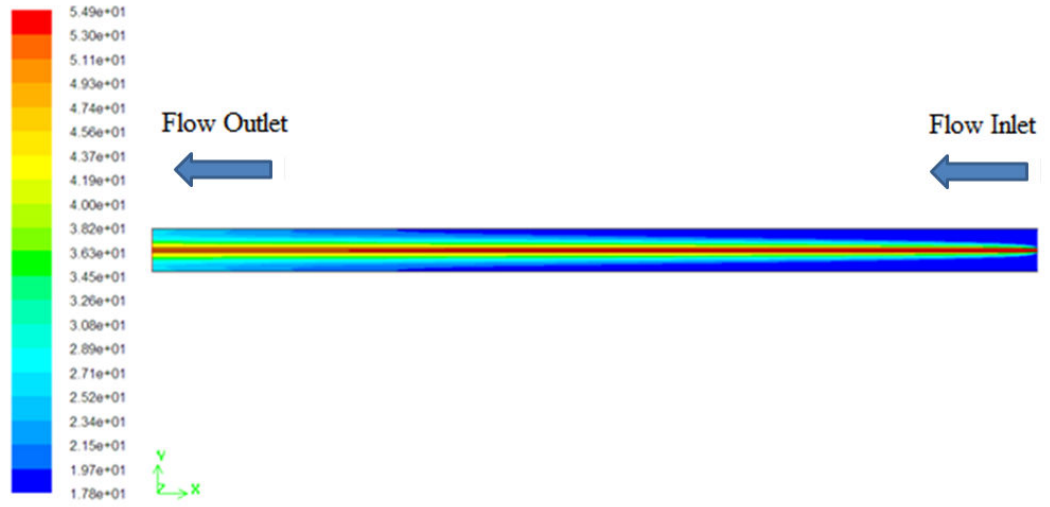
(a)



(b)



(c)



(d)

**Figure 4.15 Temperature Distribution in the Membrane Module (a) Feed Inlet Temperature at 40 °C (b) Feed Inlet Temperature at 45 °C (c) Feed Inlet Temperature at 50 °C (d) Feed Inlet Temperature at 55 °C**

## CHAPTER 5

### CONCLUSIONS AND RECOMMENDATIONS

#### 5.1 Conclusions

This research was carried out with the objective to self-fabricate, characterize, performance testing and thermal efficiency of the membrane on NaCl removal by DCMD in the experimental studies. Furthermore, the current research was also focused on the numerical simulation study conducted using CFD to investigate the membrane module temperature distribution.

In this study, six types of PVDF hollow fiber membranes were self-fabricated using dope solution with different additives such as EG, PES, SMM and LiCl. The self-fabricated membrane exhibited different membrane characteristics when different additives were added into the dope solution. The membrane morphology for the PVDF-NMP and PVDF-DMAC membrane exhibited a finger-like layer extending from the inner layer to outer surface due to the strong solvents (NMP and DMAC) used in the dope solution. In the meantime, with an addition of EG, the PVDF-EG membrane showed a finger-like structure on the inner and outer surfaces with an intermediate layer of irregular microvoids. With the addition of PES, the PVDF-EG-PES membrane showed the lowest thickness (180  $\mu\text{m}$ ) relative to other self-fabricated membrane. The most

porous membrane ( $85 \pm 1.25\%$ ) was shown in the PVDF-LiCl membrane. Lastly, the membrane with SMM additive demonstrated a good hydrophobic characteristic ( $92 \pm 0.25^\circ$ ), where it had the highest contact angle among the entire group of the membrane.

The self-fabricated membranes were applied in the NaCl rejection by DCMD process under different operating conditions. The PVDF-EG-PES membrane exhibited the best performance in terms of permeate flux relative to other self-fabricated membranes when it was evaluated at a feed inlet temperature varying from 40 to 55 °C, permeate inlet temperature at 18°C and 0.3 L/min for both permeate and feed flow rates on the permeate flux. Subsequently, the membrane was further studied for the effect of feed and permeate flow rate. The result showed that the feed and permeate flow rates exhibited a positive effect on the permeate flux.

In addition, the stability test of 20-hour continuous operation proved that the PVDF-EG-PES membrane was able to achieve a constant permeates flux, while maintaining high rejection rate throughout the longer operating period. Therefore, it could be suggested that PVDF-EG-PES membrane had the great potential to be adopted in MD process.

The thermal efficiency in this study illustrated that both feed and permeate inlet flow rates had a positive effect on the thermal efficiency which was attributed to the increase of heat transfer by vaporization of liquid compared to the heat conduction in the DCMD system as a result of higher permeate flux.

CFD numerical study was successfully simulated and the result indicated a close agreement with the experimental data. A consistent temperature distribution in the membrane module trend was found in the CFD studies.

## **5.2 Recommendations**

In addition to the tasks completed in this research project, there are several interesting topics that can be looked into in the future investigation as follows:

- To further develop self-fabricated HF membrane with higher permeate flux relative to the current study as well as with excellent membrane characteristics in the long term operating conditions.
- To integrate the current DCMD system with renewable energy such as solar power to replace the heating source of the system in order to increase the system efficiency.
- To conduct a pilot plant investigation in order to conduct the feasibility of the DCMD to be a commercially viable as seawater desalination system.

- To enhance the CFD modeling in order to study in-depth on the heat and mass transfer phenomenon in the DCMD process and to predict the permeate flux of different membranes.

## REFERENCE

Ahmad A.L., Abdulkarim A.A., Ooi B.S., Ismail S., 2013. Recent development in additives modifications of polyethersulfone membrane for flux enhancement, *Chemical Engineering Journal*, 223, pp. 246 – 267.

Ahmad A.L., Ideris N., Ooi B.S., Low S.C., Ismail A., 2012. Synthesis of polyvinylidene fluoride (PVDF) membranes for protein binding: Effect of casting thickness, *Journal of Applied Polymer Science*, 128 (5), pp. 3438 – 3445.

Ajay K.M., Sen M., Martin A.R., Pal P., 2010, Removal of arsenic from contaminated ground water by solar-driven membrane distillation, *Environment Pollution*, 188, pp. 805 – 811.

Alkhudhiri A., Darwish N., Hilal N., 2012. Membrane distillation: A comprehensive review, *Desalination*, 287, pp. 2 – 18.

Alkhudhiri A., Darwish N., Hilal N., 2013. Produced water treatment: Application of air gap membrane distillation, *Desalination*, 309, pp. 46 – 51.

Alklaibi A.M., Lior N., 2004. Membrane-distillation desalination: status and potential, *Desalination*, 171 pp. 111 – 131.

Bahmanyar A., Asghari M., Khoobi N., 2012. Numerical simulation and theoretical study on simultaneously effects of operating parameters in direct contact membrane distillation, *Chemical Engineering and Processing*, 61, pp. 42 – 50.

Banat F., Jwaied N., Rommel M., Koschikowski J., Weighaus M., 2007. Desalination by a ‘compact SMADES’ autonomous solar-powered membrane distillation unit, *Desalination*, 217, pp. 29 – 37.

Banat F., Jwaied N., Rommel M., Koschikowski J., Weighaus M., 2007. Performance evaluation of the ‘large SMADES’ autonomous desalination solar-driven membrane distillation plant in Aqaba, Jordan, *Desalination*, 217, 17 – 28.

Bonyadi S., Chung T.S., 2009. Highly porous and macrovoid-free PVDF hollow fiber membranes for membrane distillation by a solvent-dope solution co-extrusion approach, *Journal of Membrane Science*, 331, pp. 66 – 74.

Bottino A., Capannelli, Munari S., Turturro S., 1988. High performance ultrafiltration membranes cast from LiCl doped solutions, *Desalination*, 68 (2–3), pp. 167 – 177.

Bourawi M.S., Ding Z., R. Ma, Khayet M., 2006. A framework for better understanding membrane distillation separation process, *Journal of Membrane Science*, 285, pp. 4 – 29.

Essalhi M., Khayet M., 2012. Surface segregation of fluorinated modifying macromolecule for hydrophobic/hydrophilic membrane preparation and application in air gap and direct contact membrane distillation, *Journal of Membrane Science*, 417–418, pp.163 – 173.

Feng C.Y., Khulbe K.C., Matsuura T., Ismail A.F., 2013. Recent progresses in polymeric hollow fiber membrane preparation, characterization and applications, *Separation and Purification Technology*, 111, pp. 43 – 71.

Fluent 6.3 User's guide, 2006, Lebanon, Fluent Inc.

García-Payo M.C., Essalhi M., Khayet M., 2010. Effects of PVDF-HFP concentration on membrane distillation performance and structural morphology of hollow fiber membranes, *Journal of Membrane Science*, 347, pp. 209 – 219.

Ghidossi R., Veyret D., Moulin P., 2006. Computational fluid dynamics applied to membranes: State of the art and opportunities, *Chemical Engineering and Processing*, 45, pp. 437 – 454.

Hitachi High – Technologies Europe GmbH, 2014, *S3400N Scanning electron microscope*, [Online]. Available at: <http://www.hht-eu.com/cms/5405.html> [Accessed: 10<sup>th</sup> February 2014]

Hou D.Y., Wang J., Qu D., Luan Z.K., Ren X.J. 2009. Fabrication and characterization of hydrophobic PVDF hollow fiber membranes for desalination through direct contact membrane distillation, *Separation and Purification Technology*, 69, pp. 78 – 86.

Ismail A.F., Dunkin I.R., Gallivan S.L., Shilton S.J., 1999. Production of super selective polysulfone hollow fiber membranes for gas separation, *Polymer*, 40, pp. 6499 – 6506.

Khayet M., 2011. Membranes and theoretical modeling of membrane distillation: A review, *Advances in Colloid and Interface Science*, 164, pp. 56 – 88.

Khayet M., Matsuura T., 2003. Application of surface modifying macromolecules for the preparation of membranes for membrane distillation, *Desalination*, 158 pp. 1 – 56.

Khayet M., Matsuura T., 2011. *Membrane distillation principles and applications*, Amsterdam, The Netherlands: Elsevier B.V.

Lawson K.W., Lloyd D.R., 1997. Membrane distillation, *Journal of Membrane Science*, 124, pp. 1 – 25.

Li N., Fane A.G., Ho W.S., Matsuura T., 2008. *Advanced Membrane Technology and Applications*, Hoboken, New Jersey: John Wiley & Sons, Chapter 6, 7 & 12.

Liao Y., Wang R., Tian M., Qiu C.Q., Fane A.G., 2013. Fabrication of polyvinylidene fluoride (PVDF) nanofiber membranes by electro-spinning for direct contact membrane distillation, *Desalination*, 425–426, pp. 30 – 39.

Mansourizadeh A., Ismail A.F., 2010. Effect of LiCl concentration in the polymer dope on the structure and performance of hydrophobic PVDF hollow fiber membranes for CO<sub>2</sub> absorption, *Chemical Engineering Journal*, 165, pp. 980 – 988.

Obaidania S., Curcio E., Macedonio F., Profio G.I., Hinaid H.A., Drioli E., 2008. Potential of membrane distillation in seawater desalination: Thermal efficiency, sensitivity study and cost estimation, *Journal of Membrane Science*, 323, pp. 85 – 98.

Phattaranawik J., R. Jiratananon R., Fane A.G., 2003. Heat transport and membrane distillation coefficients in direct contact membrane distillation, *Journal of Membrane Science*, 212, pp. 177 – 193.

Qtaishat M., Rana D., Matsuura T., Khayet M., 2009. Effect of surface modifying macromolecules stoichiometric ratio on composite hydrophobic/hydrophilic membranes characteristics and performance in direct contact membrane distillation, *Wiley InterScience AIChE Journal*, 55 (12), pp. 3145 – 3151.

Qtaishat M., Matsuura T., Kruczek B., Khayet M., 2008. Heat and mass transfer analysis in direct contact membrane distillation, *Desalination*, 219, pp. 272 – 292.

Qu D., Wang J., Hou D.Y., Luan Z.K., Fan B., Zhao C.W., Ammonia removal by sweep gas membrane distillation, 2009. *Journal of Hazardous Materials*, 163, pp. 874 – 879.

Ramé-hart instrument co., 2013, *Ramé-hart Goniometer 250*, [Online]. Available at: <http://www.flickr.com/photos/51015268@N07/9006306993/in/set-72157634050986433> [Accessed: 10<sup>th</sup> February 2014].

Reig P., Maddocks A., Gassert F., World Resources Institute, 2013 *World's 36 Most Water-Stressed Countries* [Online]. Available at: <http://www.wri.org/blog/world%E2%80%99s-36-most-water-stressed-countries> [Accessed: 21<sup>st</sup> March 2014].

Shakaib M., Hasani S.M.F., Ahmed I., Yunus R.M., 2012. A CFD study on the effect of spacer orientation on temperature polarization in membrane distillation modules, *Desalination*, 284, pp. 332 – 340.

Sisakht M.R., Ismail A.F., Rana D., Matsuura T., 2012. A novel surface modified polyvinylidene fluoride hollow fiber membrane contactor for CO<sub>2</sub> absorption, *Journal of Membrane Science*, 415–416, pp. 221 – 228.

Smolders C.A., Franken A.C.M., 1989, Terminology for membrane distillation, *Desalination*, 72, pp. 249 – 262.

Suk D.E., Matsuura T., Park H.B., Lee Y.M., 2006. Synthesis of a new type of surface modifying macromolecules (nSMM) and characterization and testing of nSMM blended membranes for membrane distillation, *Journal Membrane Science*, 277, pp. 177 – 185.

Susanto, 2011. Towards practical implementations of membrane distillation, *Chemical Engineering and Processing*, 50, pp. 139–150.

Swenson, n.d. *Why is the ocean salty?* [Online]. Available at: [http://www.palomar.edu/oceanography/salty\\_ocean.htm](http://www.palomar.edu/oceanography/salty_ocean.htm) [Accessed: 21<sup>st</sup> March 2014].

Tang N., Zhang H.J., Wang W., 2011. Computational fluid dynamics numerical simulation of vacuum membrane distillation for aqueous NaCl solution, *Desalination*, 274, pp. 120 – 129.

Termpiyakul P., Jiraratananon R., Srisurichan S., 2005. Heat and mass transfer characteristics of a direct contact membrane distillation process for desalination, *Desalination*, 177, pp. 133 – 141.

The USGS Water Science School, 2013, *Where is the Earth's water?* [Online]. Available at: <http://ga.water.usgs.gov/edu/earthwherewater.html> [Accessed: 21<sup>st</sup> March 2014].

Tomaszewska M., 1996. Preparation and properties of flat-sheet membranes from poly(vinylidene fluoride) for membrane distillation, *Desalination*, 104, pp. 1 – 11.

Tomaszewska M., 2000. Membrane distillation - Examples of applications in technology and environmental protection, *Polish Journal of Environmental Studies*, 9, pp. 27 – 36.

Versteeg H.K., Malalasekera W., 1995. *An introduction to computational fluid dynamics : the finite volume method*, Harlow, England: Prentice Hall.

Wang K.Y., Chung T.S., Gryta M., 2008. Hydrophobic PVDF hollow fiber membranes with narrow pore size distribution and ultra-thin skin for the freshwater production through membrane distillation, *Chemical Engineering Science*, 63, pp. 2587 – 2594.

Winter D., Koschikowski J., Wieghaus M., 2011. Desalination using membrane distillation: Experimental studies on full scale spiral wound modules, *Journal of Membrane Science*, 375, pp. 104 – 112.

World health organization, 2014, *Water supply, sanitation and hygiene development* [Online]. Available at: [http://www.who.int/water\\_sanitation\\_health/hygiene/en/](http://www.who.int/water_sanitation_health/hygiene/en/) [Accessed: 21<sup>st</sup> March 2014].

Wu B., Tan X.Y., Li K., Teo W.K., 2006. Removal of 1,1,1-trichloroethane from water using a polyvinylidene fluoride hollow fiber membrane module: Vacuum membrane distillation operation, *Separation and Purification Technology*, 52, pp. 301 – 309.

Wu L.S., Sun J.F., Wang Q.R., 2006. Poly(vinylidene fluoride)/polyethersulfone blend membranes: Effects of solvent sort, polyethersulfone and polyvinylpyrrolidone concentration on their properties and morphology, *Journal of Membrane Science*, 285, pp. 290 – 298.

Xie Z.L., Duong T., Hoang M., Nguyen C., Bolto B., 2009. Ammonia removal by sweep gas membrane distillation, *Water Research*, 43, pp. 1693 – 1699.

Yang X., Yu H., Wang R., Fane A.G., 2012. Analysis of the effect of turbulence promoters in hollow fiber membrane distillation modules by computational fluid dynamic (CFD) simulations, *Journal of Membrane Science*, 415–416, pp. 758 – 769.

Yeow M.L., Liu Y.T., Li K., 2004. Morphological study of poly(vinylidene fluoride) asymmetric membranes: Effects of the solvent, additive, and dope temperature, *Journal of Applied Polymer Science*, 92, pp. 1782 – 1789.

Young T.H., Chen L.W., 1995. Pore formation mechanism of membranes from phase inversion process, *Desalination*, 103, pp. 233 – 247.

Yu H., Yang X., Wang Rong., Fane A.G., 2011. Numerical simulation of heat and mass transfer in direct membrane distillation in a hollow fiber module with laminar flow, *Journal of Membrane Science*, 384, pp. 107 – 116.

Yu H., Yang X., Wang Rong., Fane A.G., 2012. Analysis of heat and mass transfer by CFD for performance enhancement in direct contact membrane distillation, *Journal of Membrane Science*, 405– 406, pp. 38 – 47.

Yu H., Yang X., Wang Rong., Fane A.G., 2012. Analysis of heat and mass transfer by CFD for performance enhancement in direct contact membrane distillation, *Journal of Membrane Science*, 405– 406, pp. 38 – 47.

Yuliwati E., Ismail A.F., Matsuura T., Kassim M.A., Abdullah M.S., 2011. Characterization of surface-modified porous PVDF hollow fibers for refinery wastewater treatment using microscopic observation, *Desalination*, 283, pp. 206 – 213.

Zhang M.G., Nguyen Q.T., Ping Z.H., 2009. Hydrophilic modification of poly (vinylidene fluoride) microporous membrane, *Journal of Membrane Science*, 327, pp. 78 – 86.

Zhao J., Yang D.L., Zhang S.H., Jian X.G., 2007. Removal of 2,4-dichlorophenol from wastewater by vacuum membrane distillation using hydrophobic PPESK hollow fiber membrane, *Chinese Chemical Letters*, 18, pp. 1543 – 1547.

## APPENDIX A

### MEMBRANE POROSITY CALCULATION

Membrane dope solution	Porosity (%)			
	Sampling 1	Sampling 2	Sampling 3	Average
PVDF-NMP	79.22	81.28	80.32	80
PVDF-EG	62.25	59.43	57.97	60
PVDF-EG-PES	70.74	70.56	69.63	70
PVDF-SMM	83.32	82.26	82.97	83
PVDF-DMAC	69.27	69.62	70.31	70
PVDF-LiCl	84.60	84.87	86.27	85

#### Sample calculation for self-fabricated membrane (PVDF-NMP)

$$\varepsilon = \frac{(W_1 - W_2)/\rho_w}{(W_1 - W_2)/\rho_w + W_2/\rho_b} \times 100\%$$

$W_1$  is the weight of the wetted membrane

$W_2$  is the weight of dry membrane

$\rho_w$  is the specific gravity of 2-butanol ( $0.81 \text{ gcm}^{-3}$ )

$\rho_b$  is the specific gravity of PVDF ( $1.78 \text{ gcm}^{-3}$ ).

### Sampling data 1

$$W_1 = 0.0350 \text{ g} \quad W_2 = 0.0128 \text{ g} \quad \rho_W = 0.81 \text{ gcm}^{-3} \quad \rho_b = 1.78 \text{ gcm}^{-3}$$

$$\varepsilon = \frac{(0.0350 - 0.0128)/0.81}{(0.0350 - 0.0128)/0.81 + 0.0128/1.78} \times 100\% = 79.22\%$$

### Sampling data 2

$$W_1 = 0.0372 \text{ g} \quad W_2 = 0.0125 \text{ g} \quad \rho_W = 0.81 \text{ gcm}^{-3} \quad \rho_b = 1.78 \text{ gcm}^{-3}$$

$$\varepsilon = \frac{(0.0372 - 0.0125)/0.81}{(0.0372 - 0.0125)/0.81 + 0.0125/1.78} \times 100\% = 81.28\%$$

### Sampling data 3

$$W_1 = 0.0360 \text{ g} \quad W_2 = 0.0126 \text{ g} \quad \rho_W = 0.81 \text{ gcm}^{-3} \quad \rho_b = 1.78 \text{ gcm}^{-3}$$

$$\varepsilon = \frac{(0.0360 - 0.0126)/0.81}{(0.0360 - 0.0126)/0.81 + 0.0126/1.78} \times 100\% = 80.32\%$$

Average porosity for self-fabricated membrane (PVDF-NMP)

$$\varepsilon = \frac{79.22 + 81.28 + 80.32}{3} = 80.27\% \approx 80\%$$

## APPENDIX B

### MEMBRANE CONTACT ANGLE MEASUREMENT

Membrane dope solution	Contact angle (°)
PVDF-NMP	88
PVDF-EG	82
PVDF-EG-PES	85
PVDF-SMM	92
PVDF-DMAC	76
PVDF-LiCl	76

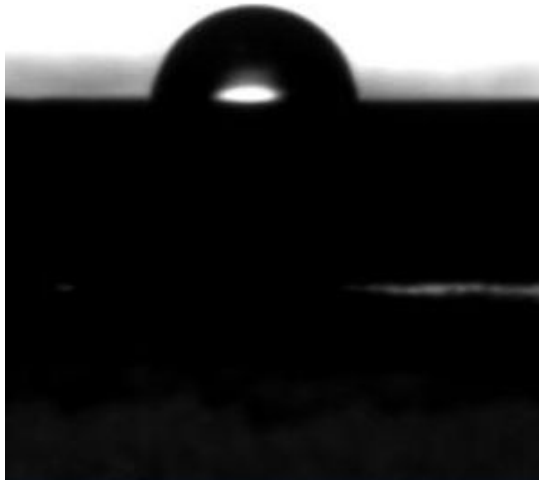


Figure B1 Contact angle image of PVDF-NMP using sessile drop technique

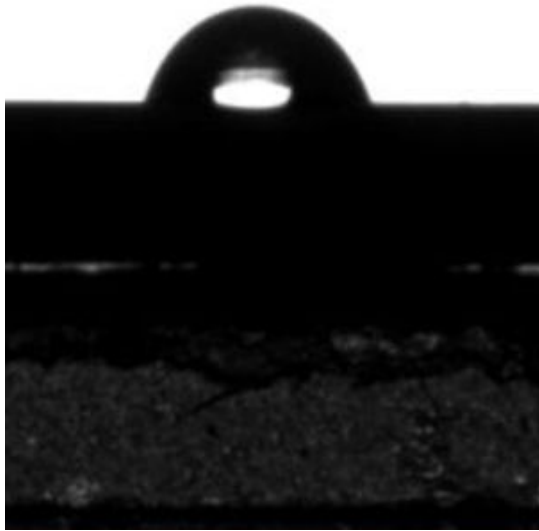


Figure B2 Contact angle image of PVDF-EG using sessile drop technique

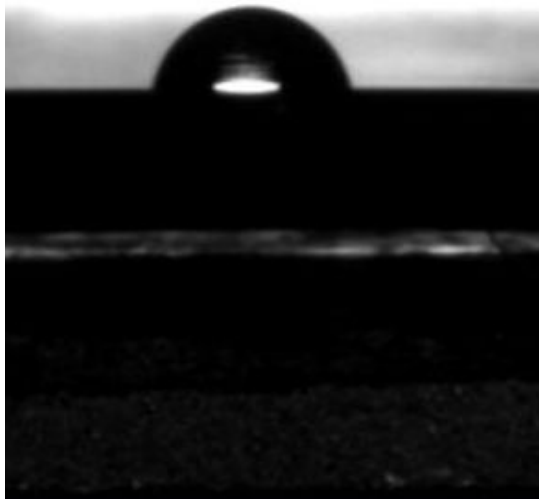


Figure B3 Contact angle image of PVDF-EG-PES using sessile drop technique

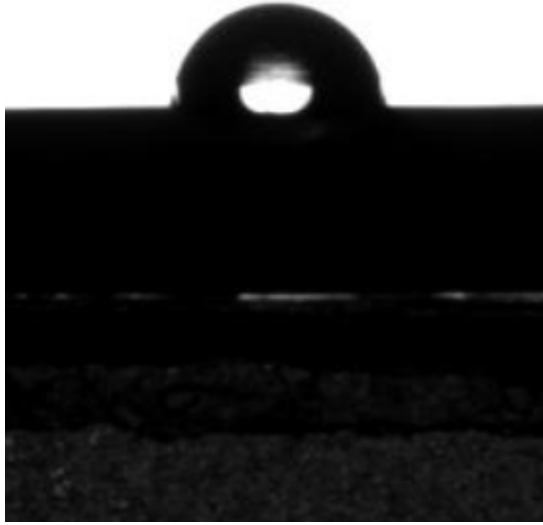


Figure B4 Contact angle image of PVDF-SMM using sessile drop technique

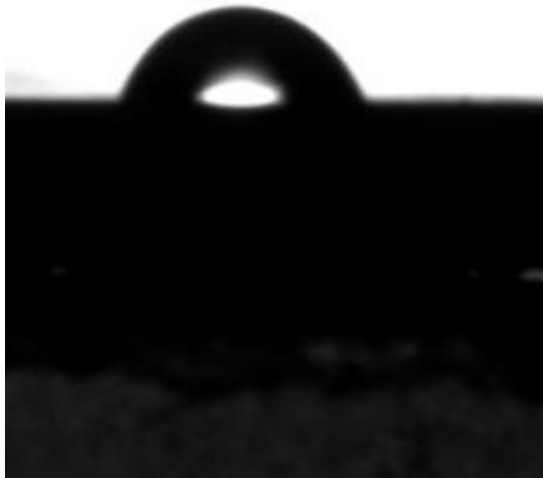


Figure B5 Contact angle image of PVDF-DMAC using sessile drop technique

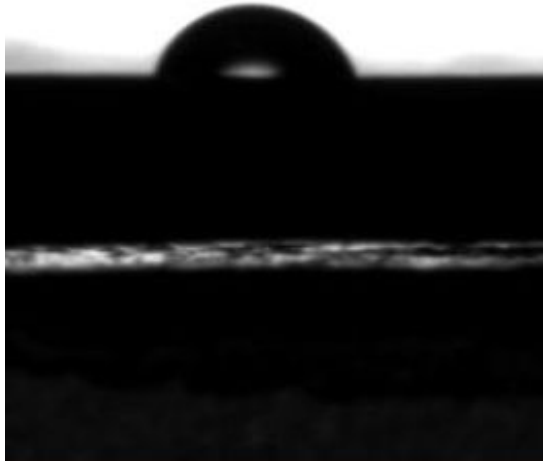


Figure B6 Contact angle image of PVDF-LiCl using sessile drop technique

## APPENDIX C

### MEMBRANE LIQUID ENTRY PRESSURE MEASUREMENT

Membrane dope solution	Liquid entry pressure (bar)			
	Sampling 1	Sampling 2	Sampling 3	Average
PVDF-NMP	3.4	3.5	3.5	3.5
PVDF-EG	3.8	3.7	3.7	3.7
PVDF-EG-PES	4.0	4.0	3.9	4.0
PVDF-SMM	3.0	3.1	3.0	3.0
PVDF-DMAC	2.5	2.6	2.6	2.6
PVDF-LiCl	2.8	2.7	2.8	2.8

#### Sample calculation for self-fabricated membrane (PVDF-NMP)

Average liquid entry pressure, LEP for self-fabricated membrane (PVDF-NMP)

$$LEP = \frac{3.4 + 3.5 + 3.5}{3} = 3.4667 \text{ bar} \approx 3.5 \text{ bar}$$

## APPENDIX D

### EFFECT OF TEMPERATURE ON DCMD PERFORMANCE

Average Temperature (°C)		Average Permeate Flux (kg/m <sup>2</sup> hr)					
Feed side	Permeate side	PVDF-NMP	PVDF-EG	PVDF-EG-PES	PVDF-SMM	PVDF-DMAC	PVDF-LiCl
40	18	1.001	1.877	2.954	1.917	1.528	1.958
45	18	1.884	2.859	3.921	2.959	2.092	2.595
50	18	3.611	4.335	4.842	4.502	2.938	3.622
55	18	5.375	5.320	6.435	6.232	4.043	4.913

## APPENDIX E

### EFFECT OF FLOW RATE ON DCMD PERFORMANCE

Effect of feed flow rate on DCMD performance using PVDF-EG-PES membrane

Average Temperature (°C)		Flow rate (l/min)		Average Permeate Flux (kg/m <sup>2</sup> hr)
Feed side	Permeate side	Feed side	Permeate side	
55	18	0.10	0.30	2.923
55	18	0.20	0.30	3.177
55	18	0.30	0.30	6.012
55	18	0.40	0.30	6.438
55	18	0.50	0.30	8.631
55	18	0.60	0.30	9.230

Effect of permeate flow rate on DCMD performance using PVDF-EG-PES membrane

Average Temperature (°C)		Flow rate (l/min)		Average Permeate Flux (kg/m <sup>2</sup> hr)
Feed side	Permeate side	Feed side	Permeate side	
55	18	0.60	0.10	7.881
55	18	0.60	0.20	8.600
55	18	0.60	0.30	9.230
55	18	0.60	0.40	10.160
55	18	0.60	0.50	12.830
55	18	0.60	0.60	14.120

## APPENDIX F

### MEMBRANE STABILITY TEST

Membrane stability test under feed inlet temperature at 55°C, permeate inlet temperature at 18°C, feed and permeate inlet flow rate at 0.3 L/min respectively using PVDF-EG-PES membrane

Time (hour)	Permeate flux (kg/m <sup>2</sup> hr)	Difference from mean (%)	Rejection rate	Difference from mean (%)
1	7.02	-9.84	99.96	-0.28
2	6.73	-5.18	99.90	-0.22
3	6.47	-1.16	99.85	-0.17
4	6.31	1.31	99.84	-0.16
5	6.79	-6.20	99.84	-0.16
6	6.25	2.30	99.79	-0.11
7	6.62	-3.53	99.73	-0.06
8	6.07	5.07	99.68	0.00
9	6.45	-0.81	99.64	0.04
10	6.75	-5.52	99.60	0.08
11	6.48	-1.27	99.56	0.12
12	6.61	-3.35	99.57	0.11
13	5.89	7.93	99.55	0.13
14	6.17	3.57	99.56	0.12
15	6.44	-0.72	99.59	0.09
16	6.08	4.95	99.60	0.08
17	6.43	-0.55	99.59	0.09
18	6.17	3.51	99.60	0.08
19	6.33	1.01	99.61	0.07
20	5.85	8.49	99.62	0.06

Membrane stability test under feed inlet temperature at 55°C, permeate inlet temperature at 18°C, feed and permeate inlet flow rate at 0.6 L/min respectively using PVDF-EG-PES membrane

Time (hour)	Permeate flux (kg/m <sup>2</sup> hr)	Difference from mean (%)	Rejection rate	Difference from mean (%)
1	14.36	6.02	99.93	-1.66
2	15.36	-0.53	99.91	-1.53
3	16.35	-7.01	99.87	-1.22
4	16.41	-7.40	99.83	-0.99
5	15.69	-2.67	99.85	-1.12
6	15.62	-2.23	99.81	-0.85
7	15.34	-0.37	99.79	-0.74
8	15.97	-4.52	99.71	-0.21
9	14.33	6.25	99.66	0.14
10	14.48	5.21	99.51	1.10
11	14.98	1.95	99.44	1.58
12	15.81	-3.50	99.46	1.46
13	15.60	-2.11	99.33	2.32
14	15.32	-0.28	99.34	2.24
15	15.15	0.86	99.38	1.93
16	14.49	5.20	99.41	1.75
17	14.39	5.83	99.40	1.84
18	15.61	-2.18	99.33	2.32
19	15.44	-1.06	99.36	2.10
20	14.89	2.55	99.42	1.73

## APPENDIX G

### DATA INPUT IN FLUENT® SOFTWARE

#### Setting of governing equation and boundary conditions

FLUENT

Version: 2d, pbns, lam (2d, pressure-based, laminar)

Release: 6.3.26

Title:

Models

-----

Model	Settings
Space	2D
Time	Steady
Viscous	Laminar
Heat Transfer	Enabled
Solidification and Melting	Disabled
Radiation	None
Species Transport	Disabled
Coupled Dispersed Phase	Disabled
Pollutants	Disabled
Pollutants	Disabled
Soot	Disabled

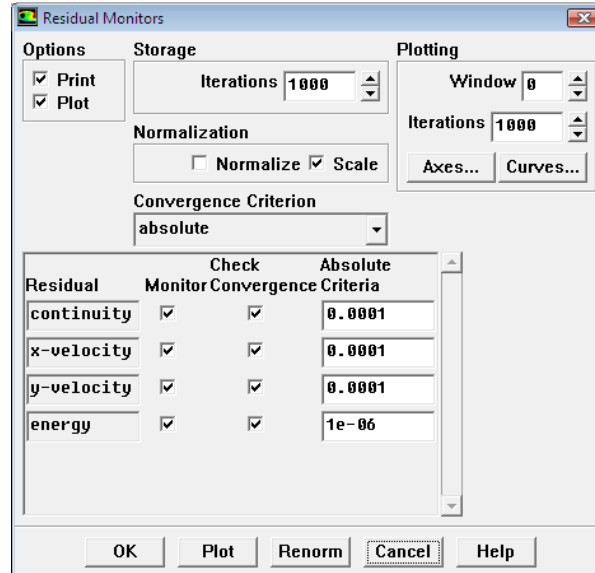
Boundary Conditions

-----

Zones

Name	id	type
Water	2	fluid
membrane-shadow	9	wall
hot_out	3	pressure-outlet
cold_out	4	pressure-outlet
hot_in	5	velocity-inlet
cold_in	6	velocity-inlet
membrane	7	wall
module_wall	8	wall

## Convergence criterion



The image shows a software dialog box titled "Residual Monitors". It is divided into three main sections: Options, Storage, and Plotting. The Options section has checkboxes for "Print" and "Plot", both of which are checked. The Storage section includes a field for "Iterations" set to 1000, a "Normalization" section with "Normalize" unchecked and "Scale" checked, and a "Convergence Criterion" dropdown menu set to "absolute". The Plotting section has a "Window" field set to 0, another "Iterations" field set to 1000, and buttons for "Axes..." and "Curves...". Below these sections is a table with columns for "Residual", "Check Monitor", "Check Convergence Criteria", and "Absolute". The table lists four residuals: continuity, x-velocity, y-velocity, and energy, each with all three check boxes checked and an associated absolute value. At the bottom of the dialog are buttons for "OK", "Plot", "Renorm", "Cancel", and "Help".

Residual	Check Monitor	Check Convergence Criteria	Absolute
continuity	<input checked="" type="checkbox"/>	<input checked="" type="checkbox"/>	0.0001
x-velocity	<input checked="" type="checkbox"/>	<input checked="" type="checkbox"/>	0.0001
y-velocity	<input checked="" type="checkbox"/>	<input checked="" type="checkbox"/>	0.0001
energy	<input checked="" type="checkbox"/>	<input checked="" type="checkbox"/>	1e-06

## APPENDIX H

### LIST OF PUBLICATION

#### 1.0 Journal Paper

1. K.C. Chong, S.O. Lai, K.M. Lee, W.J. Lau, A.F. Ismail, B.S. Ooi, Characteristic and performance of polyvinylidene fluoride membranes blended with different polymeric additives in direct contact membrane distillation, *Desalination and Water Treatment*, (2014) 1 – 9, in article (Thomsom ISI indexed journal).
2. K.C. Chong, S.O. Lai, W.J. Lau, B.S. Ooi, Preparation, characterization and performance of polyvinylidene fluoride membrane for sodium chloride rejection in direct contact membrane distillation, *Materials Research Innovation*, Accepted (Thomsom ISI indexed journal).
3. S.O. Lai, K.C. Chong, K.M. Lee, W.J. Lau, B.S. Ooi, Characteristic and performance of polyvinylidene fluoride membranes blended with lithium chloride in direct contact membrane distillation, *Jurnal Teknologi*, 69:9 (2014) 93 – 97 in article (Scopus/EI indexed journal).
4. K.C. Chong, S.O. Lai, B.S. Ooi, Recent progress in membrane distillation, *Jurnal Teknologi*, 70:2 (2014) 97 – 103 in article (Scopus/EI indexed journal).
5. K.C. Chong, S.O. Lai, K.M. Lee, W.J. Lau, B.S. Ooi, Performance of polyvinylidene fluoride hollow fiber membrane in membrane distillation,

*Advance Materials Research*, 795 (2013) 137 – 140, in article (Scopus/EI indexed journal).

## **2.0 Conference**

1. K.C. Chong, S.O. Lai, K.M. Lee, B.S. Ooi, W.J. Lau, A study of computational fluid dynamics on membrane module in membrane distillation, *1<sup>st</sup> International Conference on Innovation, Management and Technology Research 2012, Malaysia*.
2. K.C. Chong, S.O. Lai, K.M. Lee, W.J. Lau, B.S. Ooi, Performance of polyvinylidene fluoride hollow fiber membrane in membrane distillation, *The 2<sup>nd</sup> International Conference on Sustainable Materials Engineering 2013, Malaysia*.
3. S.O. Lai, K.C. Chong, K.M. Lee, W.J. Lau, B.S. Ooi, Characteristic and performance of polyvinylidene fluoride membranes blended with lithium chloride in direct contact membrane distillation, *11<sup>th</sup> International on Membrane and Science Technology 2013, Malaysia*.
4. K.C. Chong, S.O. Lai, W.J. Lau, B.S. Ooi, Preparation, characterization and performance of polyvinylidene fluoride membrane for sodium chloride rejection in direct contact membrane distillation, *1<sup>st</sup> International Conference on the Science and Engineering of Materials 2013*.